POWER PLANT
RESEARCH DIVISION

EFFECT OF RADIAL DISTANCE FROM HIGH EXPLOSIVE ON BREAKUP CHARACTERISTICS OF SOLID MATERIALS IN SPHERICAL BOMBLETS

Contract DA-18-108-405-CML-829

Special Report 0395-04(16)SP / February 1963 / Copy 38

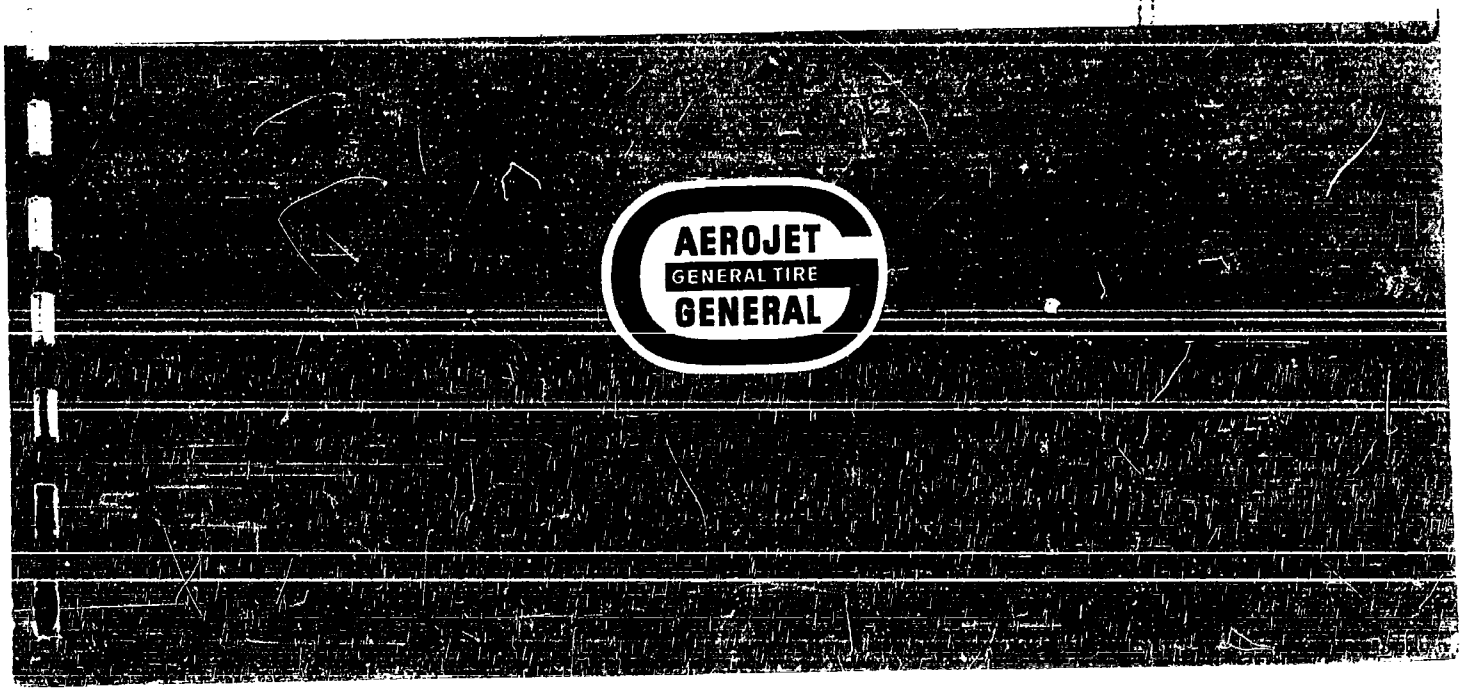

ABSTRACT

This special report describes an experimental method for determining the effect of radial distance from an explosive charge on the net size reduction of solid particles in a spherical CW bomblet. Data showing the effect of position in bomblet, size of bomblet, agent-to-explosive mass ratio and shock amplification on final breakup are presented.

Methods for chemical analysis of both the inorganic and organic materials used as agents (simulants) and tracers are presented.

CONTENTS

ILLUSTRATIONS

ILLUSTRATIONS

TABLES

1. INTRODUCTION

The dissemination of chemical warfare agents by various explosive devices was studied by numerous investigators (References 1 through 7). A spherical device containing the agent surrounding a central explosive burster charge was chosen for this study because of its simplicity, and uniform geometry. Most investigations to date on the explosive dissemination of solid and liquid materials were designed around parametric studies of initial states and final aerosol cloud measurements. Studies such as those conducted by Buck at CRDL (References 4 and 7) and by the Stanford Research Institute (Reference 1) have produced information on aerosol particle-size distribution as functions of agent-to-burster weight ratios, length-to-diameter ratios (in cylindrical devices), gross size of bomblet, etc. Some theoretical consideration was given to the mechanisms involved in the production of aerosols by explosive devices (References 5 and 8) but not enough experimental work was conducted to confirm these theoretical approaches.

In order to pursue further work of either a theoretical or practical nature in the area of explosive dissemination, experiments must be specifically designed to study the intervening processes between initial and final states.

In the case of spherical bombs, there are three general regions of interest. The first, neglecting the structural members, is the region closest to the explosive charge. In this region, both the shock and thermal effects from the explosive detonation products should be greater. Proceeding outward is the intermediate region which is subjected mostly to shock compression, with less thermal effect, and finally, the outer region which is subjected to shock compression and tensile effects caused by reflections from the outer boundary of the device and aerodynamic effects as the material moves out through the surrounding atmosphere. The difference in behavior of particulate materials located in these various regions is the subject of this investigation.

2. METHOD OF DETERMINING RADIAL EFFECTS

2.1 EXPERIMENTAL PROCEDURE

Spherical devices were constructed (Figure 1) with concentric spherical layers which contained inert potassium alum (Mallinckrodt No. 3216) or tracer chrome alum (Mallinckrodt No. 4496). These materials were selected because of similar physical properties and the ease of analysis of the chromium ion from the tracer. A relatively uniform size range of these materials was obtained by isolating a sieve fraction between 20 and 32 mesh. The comparison of properties of these two materials is given in Table 1.

All of the structural components of the bomblets were made of 0.010-in.-thick extruded cellulose acetate sheet shaped on a vacuum-forming apparatus.

The devices were fired in the center of a 21.5-ft-dia by 24-ft-high aerosol test chamber. The resultant aerosol clouds were sampled as follows: Twenty-four trays, covering 11.3% of the total chamber floor area, were left in place for three hours after the firing. In most cases at least 95% of the disseminated material had fallen out after this time making the tray samples representative of the cloud material. The material collected on these floor trays was weighed and sieved through a series of screens with openings ranging from 833 μ to 37 μ. The salt collected on each sieve was weighed and analyzed for chromium (see Appendix A). A particle-size-distribution curve was plotted for both total salt and chrome alum for each shot based on these weights. Millipore filter samples were taken six feet from the chamber wall and 12 ft above the floor at various time intervals during the course of the first half hour after detonation. The Millipore samples were weighed and chemically analyzed for chromium. From this filter data mass-decay curves can be plotted from which particle-size distributions may be calculated.

Test results described herein are divided into two groups: (1) overall results for the entire salt content of the bomb, and (2) results for the tracer material. Gross results for the entire salt charge were determined by weighing sieve cuts and Millipore samples. Tracer results were determined by analyzing all of the samples (i.e., sieve cuts and millipore filters) chemically for the tracer and running the same calculations on tracer weights that were run on the gross salt weights. Material balances were calculated by weighing the salt recovered on the trays and multiplying this weight by 8.85.

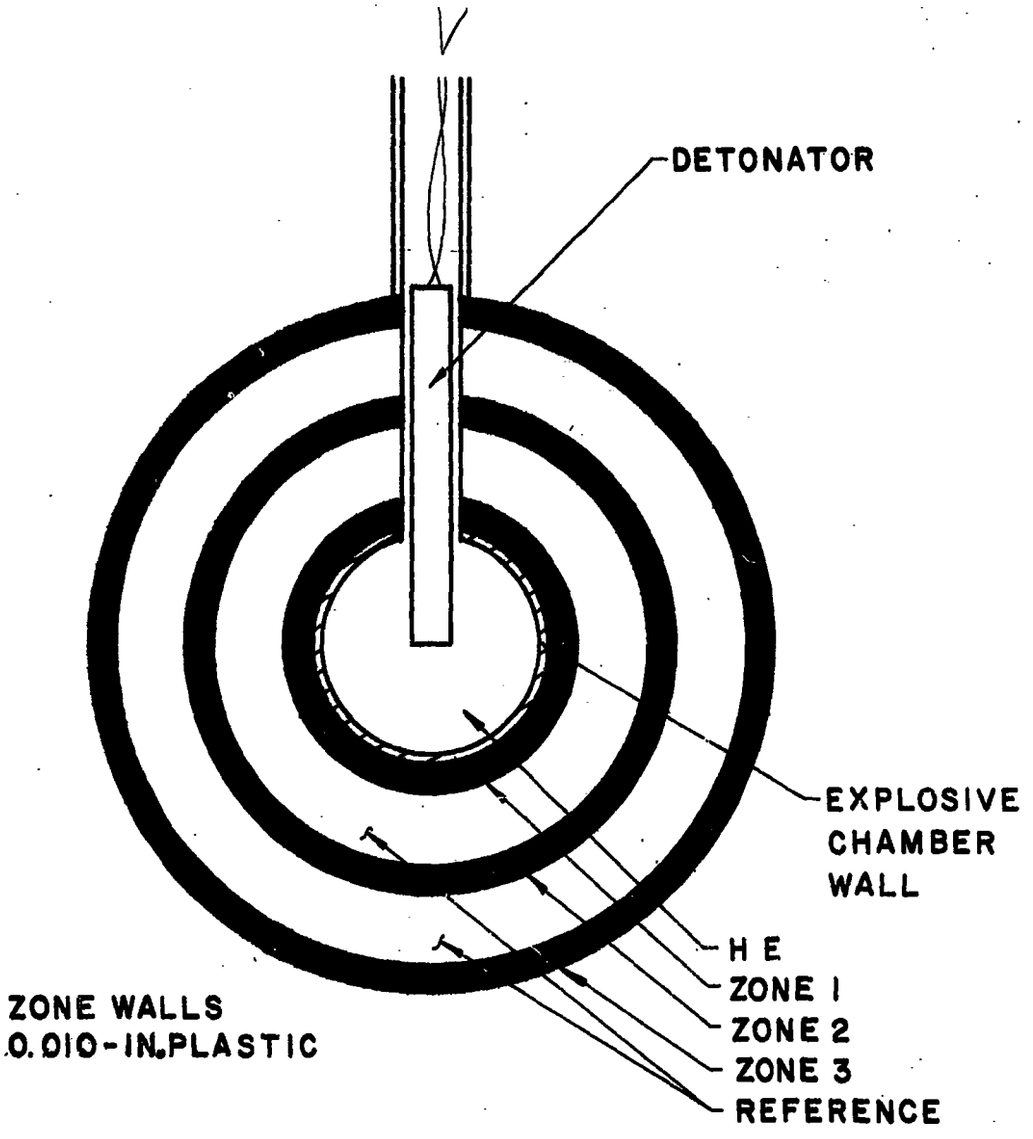

Figure 1. Spherical Explosive Dissemination Device.

Table 1. Properties of Chrome and Potassium Alums.

Designation	Chrome Alum	Potassium Alum
Formula	$K\ Cr(SO_4)_2:12H_2O$	$K\ Al(SO_4)_2:12H_2O$
Specific Gravity	1.83	1.76
Melting Point	89°C	92°C
Specific Heat	0.265 cal/gm (15°C)	0.324 cal/gm (15°C)
Formula Weight	499.4	474.4
Refractive Index	1.4814	1.4564
Crystal System	Cubic	Cubic
Color	Purple	White
Crystal Habit	Octahedral	Octahedral
Use in Munition	Tracer	Inert

Composition C-4 was the explosive used in these tests. This explosive is a mixture of 91% RDX (cyclotrimethylenetrinitramine), 2.1% polyisobutylene, 1.6% motor oil, and 5.3% di-(2-ethylhexyl) sebacate. It was [illegible] and centrally detonated with a du Pont E-83 detonator.

2.2 PRELIMINARY EXPERIMENTAL RESULTS WITH INORGANIC SALTS

The first experiments were generally to determine whether any difference in behavior of the material was noted in the three general zones as illustrated in Figure 2. The agent-to-burster weight ratio of these tests was on the order of 28:1. Results from these tests are shown in Table 2.

Tests were conducted in which the bomblets contained either all tracer or all inert material. These tests were 10, 11, and 13 (Table 2). These shots were made to compare the similarity between tracer and inert agent, the assumption being that the tracer and agent would each duplicate the breakup characteristics of the other. If this assumption were correct the final breakup of the total salt content of the bomblets, as characterized by mass median diameter (MMD), should be the same for all cases, regardless of the position of the tracer. Figure 3 indicates the slight deviation from this ideal behavior for the average values of total salt content for Tests 2 through 7.

Plotting the data for tracer breakup vs radial distance from the explosive charge surface gave the graph illustrated in Figure 4. The data recorded on Figure 4 indicate that the breakup of salt is greatest in the region immediately adjacent to the high explosive, diminishes with distance, and then increases again at the outer surface of the device.

To qualitatively eliminate the possibility of the increased breakup in the outermost section of the bomblet being due to impaction on the aerosol chamber walls, a standard concentric sphere device loaded with chrome alum was fired. Petri dishes filled with Dow-Corning silicone grease, Type 4, smoothed on top, were taped to the walls of the chamber at the same height as the bomb. Penetrations of the grease by particles of the chrome alum indicate the force with which the particles impact the chamber walls. Eight areas around the tank wall were covered with the grease dishes. Typical dishes recovered after tests are shown in Figure 5. Of the particles striking the surface, ~2% (by number) penetrated the grease; an insignificant fraction of these particles penetrated to any appreciable depth. These results indicate that secondary breakup by impaction on the walls of the chamber is probably of minor, if any, importance in these tests.

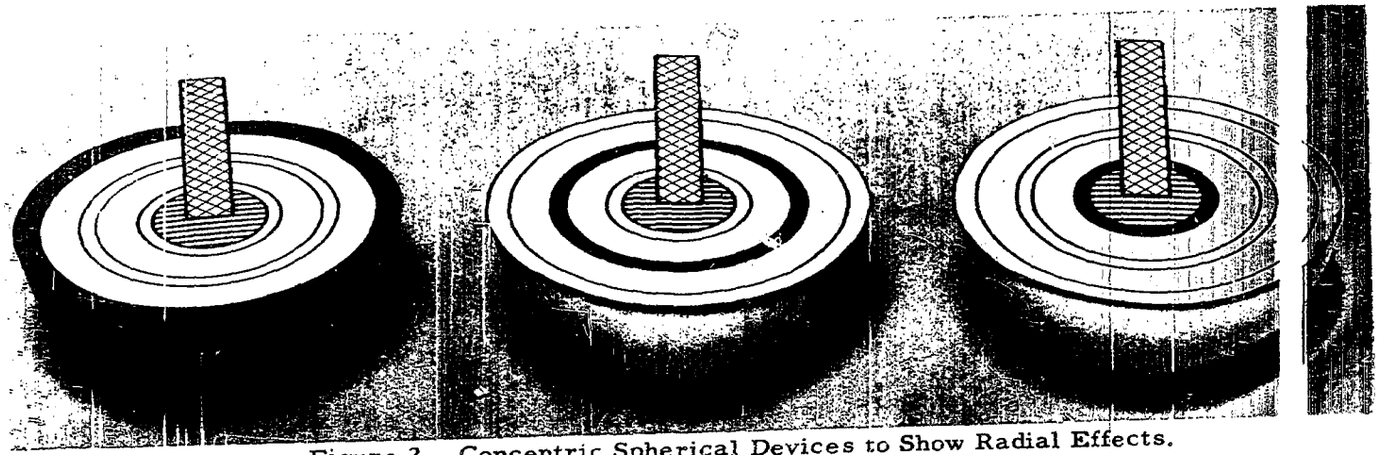

Figure 2. Concentric Spherical Devices to Show Radial Effects.

Table 2. Experimental Data for Concentric Sphere Series (Alum). (Group 1)

Test	Tracer-Charge Distance, Average (in.)	Initial MMD (μ)	Total Salt Final MMD (μ)		Tracer Final MMD (μ)		Material Balance (%)	
			Each Test	Average	Each Test	Average	Total Salt	Tracer
2	0.07	665	200	205.0	150	126.5	96.0	67.1
3	0.07		210		103		94.0	59.8
4	0.57		255	250.0	442	435.5	99.6	87.8
5	0.57		245		429		89.4	85.9
6	1.07		176	185.5	192	188.5	116.5	80.5
7	1.07		195		185		99.8	78.8
10	All Inert		217	217.0	---	---	87.2	----
11	All Tracer		287	275.0	287	275.0	85.4	85.4
13	All Tracer		263		263		81.5	81.5

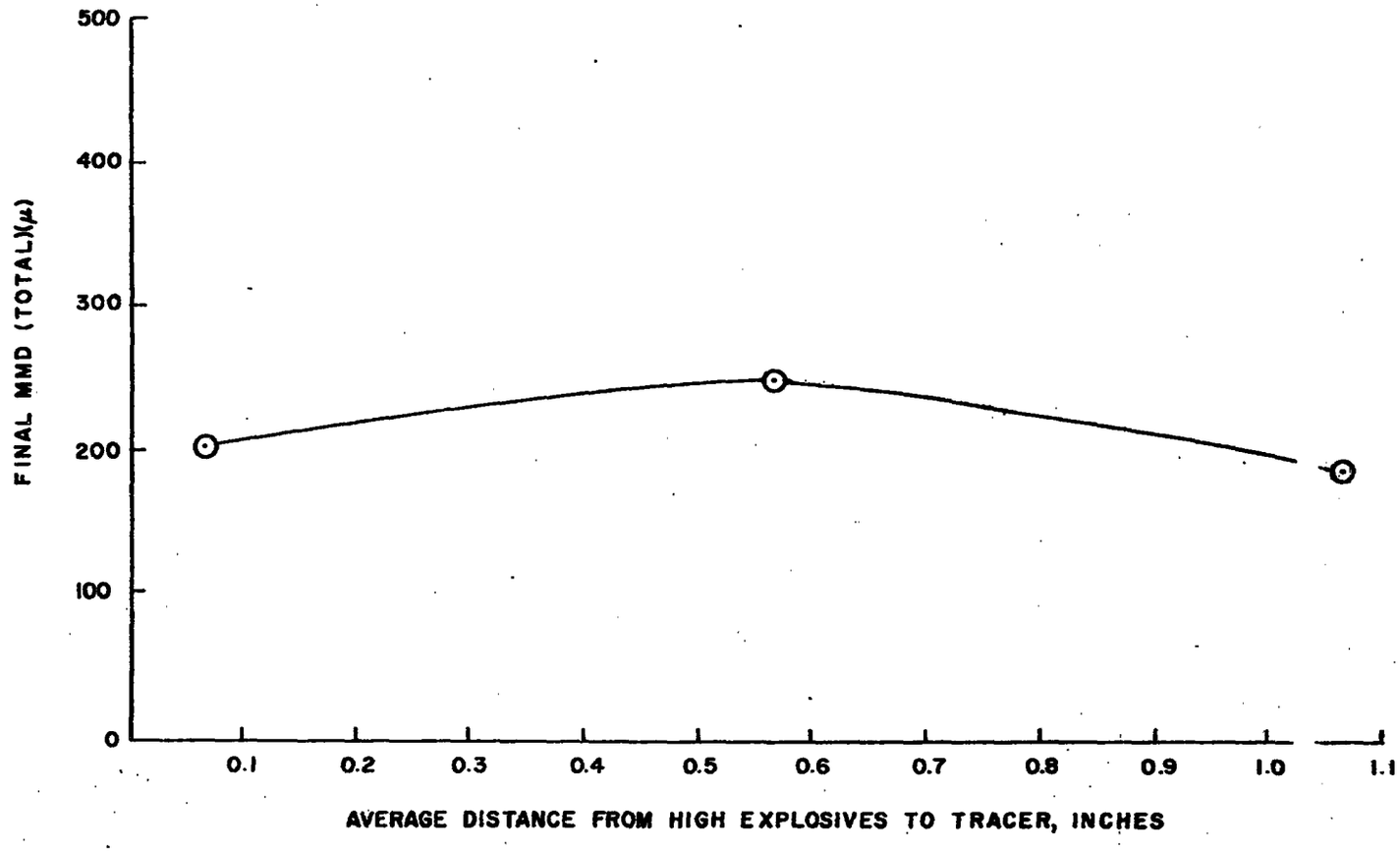

Figure 3. Variation of Resultant Gross MMD With Tracer Positions.

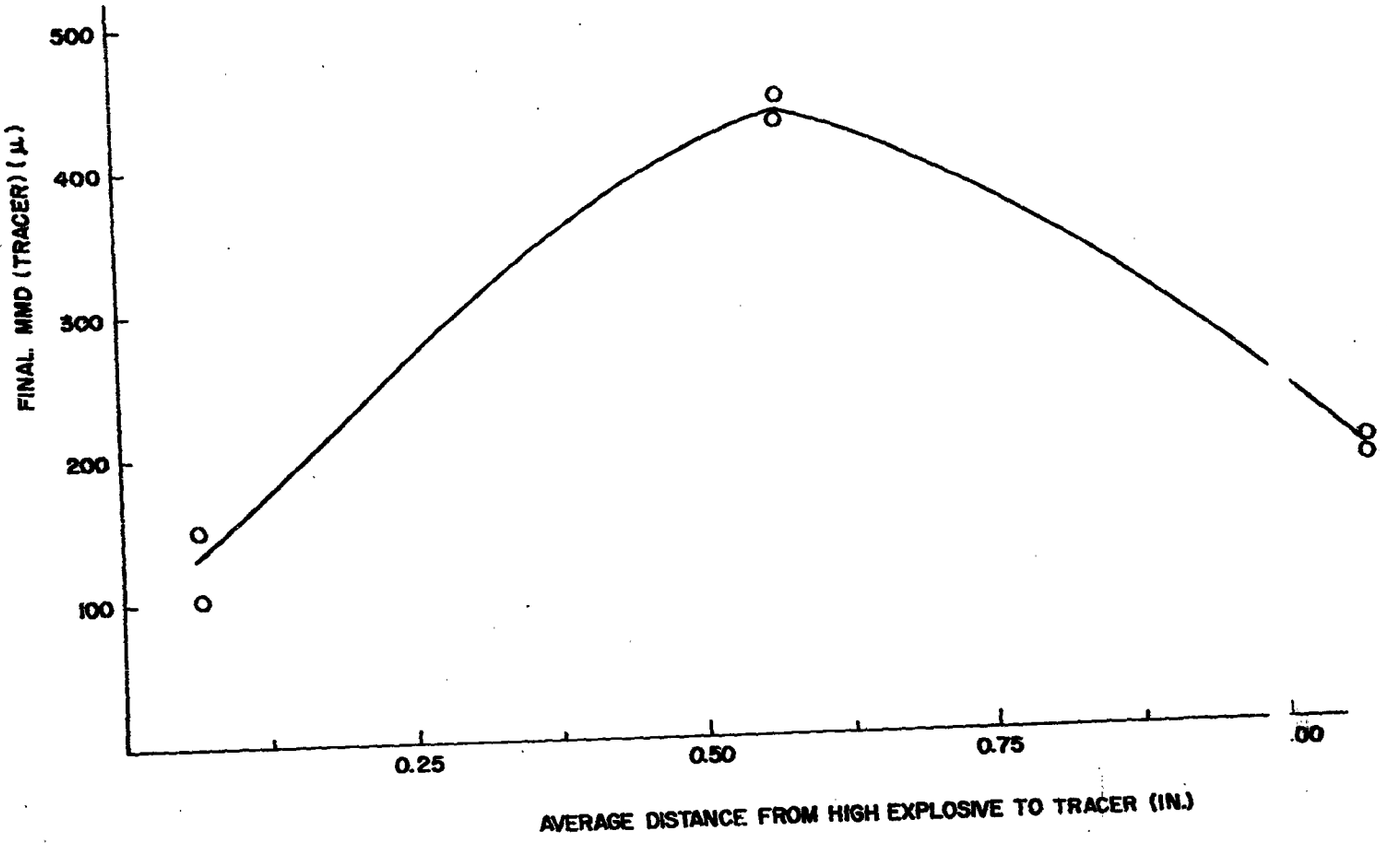

Figure 4. Plot of Tracer Breakup vs Radial Distance From Charge.

(Side View)

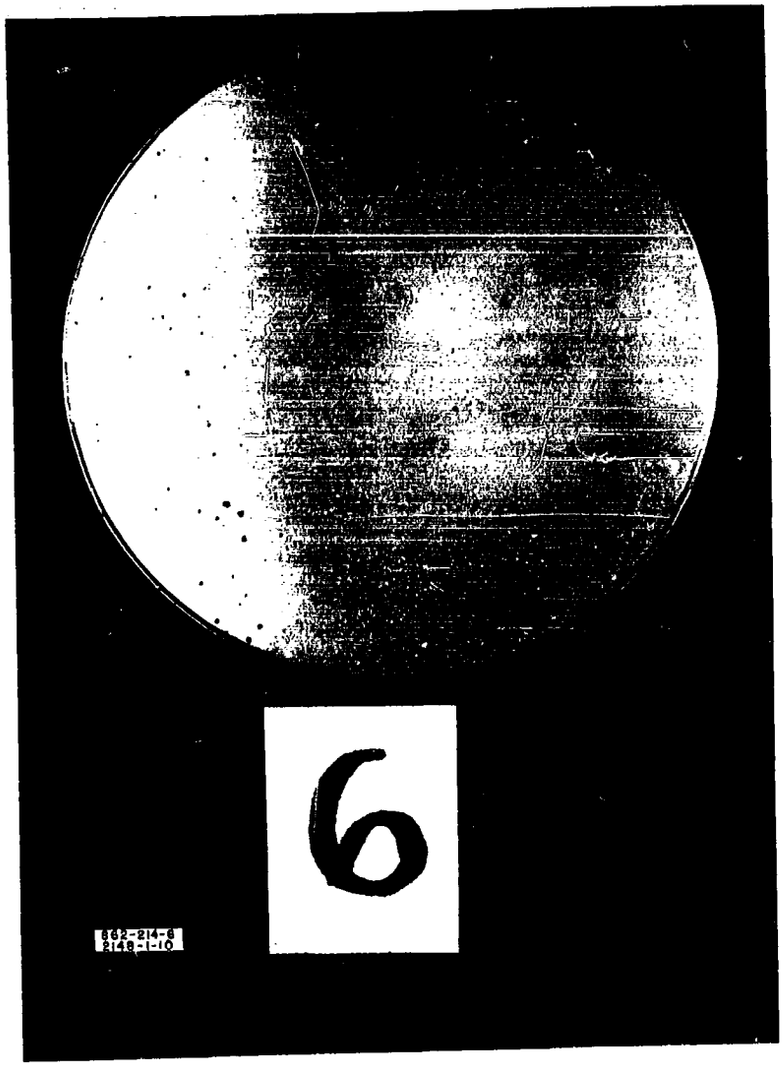

(Top View)

Figure 5. Silicone Grease Impaction Sampler.

3. DETAILED EXPERIMENTAL RESULTS

3.1 EFFECT OF VARYING TRACER POSITION

3.1.1 Inorganic Salts

The dual breakup effect noted in Table 2 was confirmed by running additional experiments in which the zones previously loaded with only inert potassium alum were loaded with the tracer. In addition, two tests were conducted using 0.060-in.-thick explosive chamber walls instead of the usual 0.010-in. walls. These are Tests 8 and 9 in Table 3 and were tested to see whether additional thermal insulation of the explosive products would result in a change in final size distribution due to a thermal effect of the hot detonation gases. Results from all of these additional tests are shown in Table 3. The combined data from all tests listed in Tables 2 and 3 are illustrated in Figure 6.

3.1.2 Organic Compounds

The apparently reproducible behavior of the breakup patterns of inorganic alums raises the question of whether the behavior of organic materials (which closely simulate the properties of CW agents) would be similar. To study this behavior, a series of concentric sphere experiments were conducted similar to those already described except that organic materials rather than alums were used in the devices. The use of ascorbic acid as the inert filler and calcium ascorbate as tracer was considered but rejected when it was found experimentally that these materials, after explosive dissemination, became hygroscopic. Anthraquinone was therefore chosen as the inert solid with p-aminobenzoic acid as the tracer. These materials had somewhat similar properties, could be readily assayed, and were in a size range typically resulting from large-scale organic production methods, such as those probably used with active agents. Properties of these materials are given in Table 4. Particle-size distributions of these materials as used were determined by a micromerograph and are given in Figures 7 and 8.

Table 3. Experimental Data for Concentric Sphere Series (Alum). (Group 2)

Test	Tracer-Charge Distance, Average (in.)	Initial MMD (μ)	Total Salt Final MMD (μ)		Tracer Final MMD (μ)		Material Balance (%)	
			Each Test	Average	Each Test	Average	Total Salt	Tracer
8	0.12	665	225	225.0	117	108.5	101.5	159.0
9	0.12		225		100		117.0	194.0
14	0.32		167	163.5	212	178.0	83.3	70.5
16	0.32		160		144		70.0	22.6
15	0.82		236	233.4	262	277.5	82.4	34.2
12	0.82		231		293		93.9	65.8

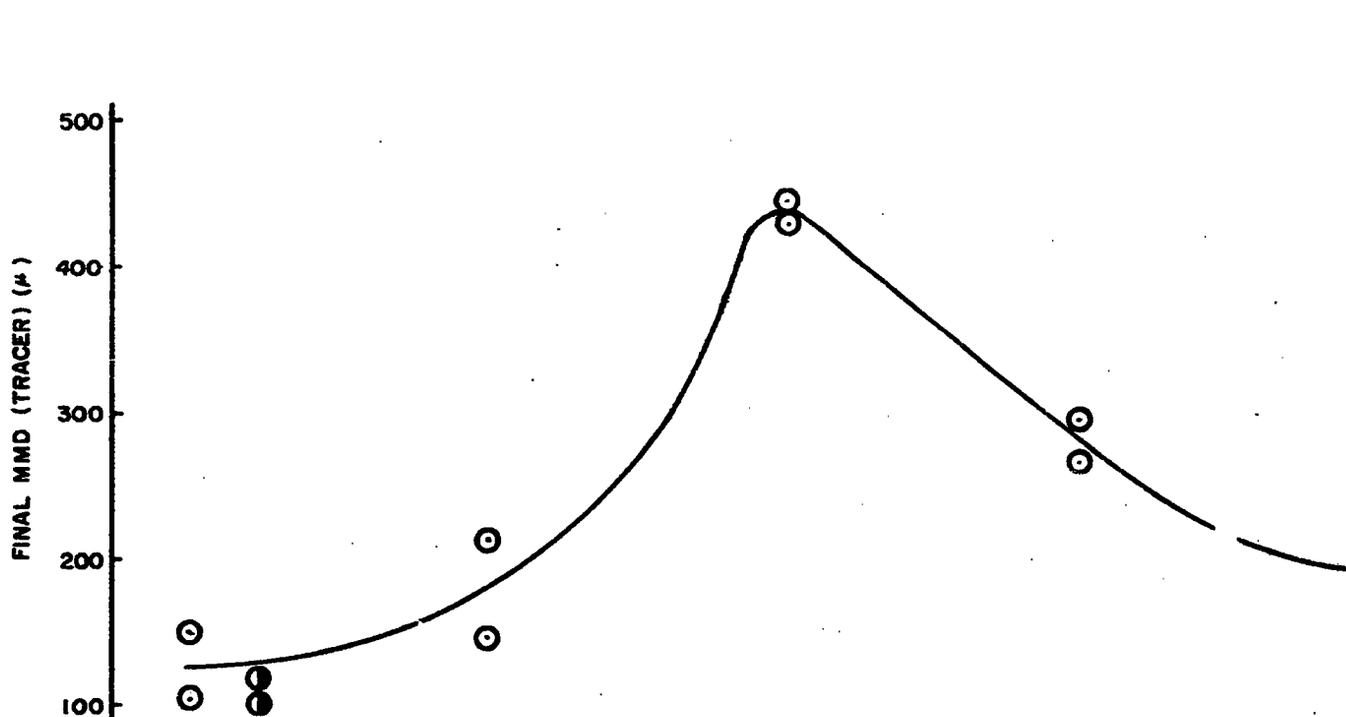

2148-8-1 Figure 6. Particle Size of Tracer vs Radial Distance From Explosive Charge.

Table 4. Properties of Anthraquinone and p-Aminobenzoic Acid.

Designation	Anthraquinone	p-Aminobenzoic Acid
Formula	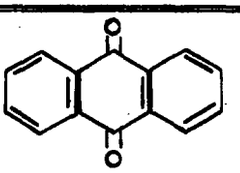	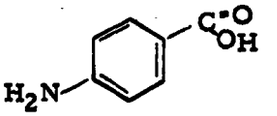
Specific Gravity	1.4	1.5
Melting Point	286°C	186°C
Specific Heat	0.258 cal/g(15°C)	0.287 cal/g(15°C)
Formula Weight	208.06	137.06
Color	Yellow	Yellow
Use In Munition	Inert	Tracer

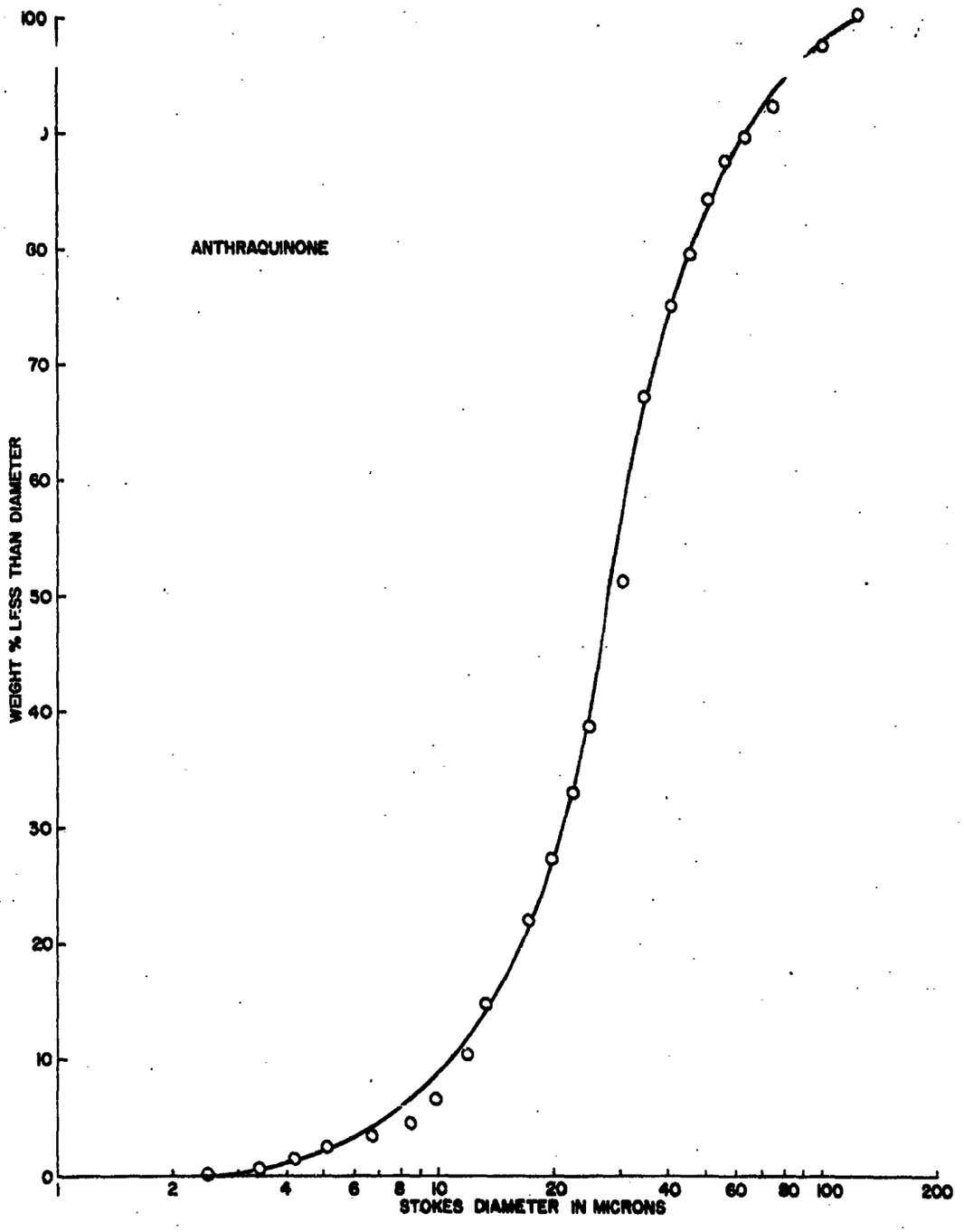

Figure 7. Particle-Size Distribution of Starting Material (Anthraquinone).

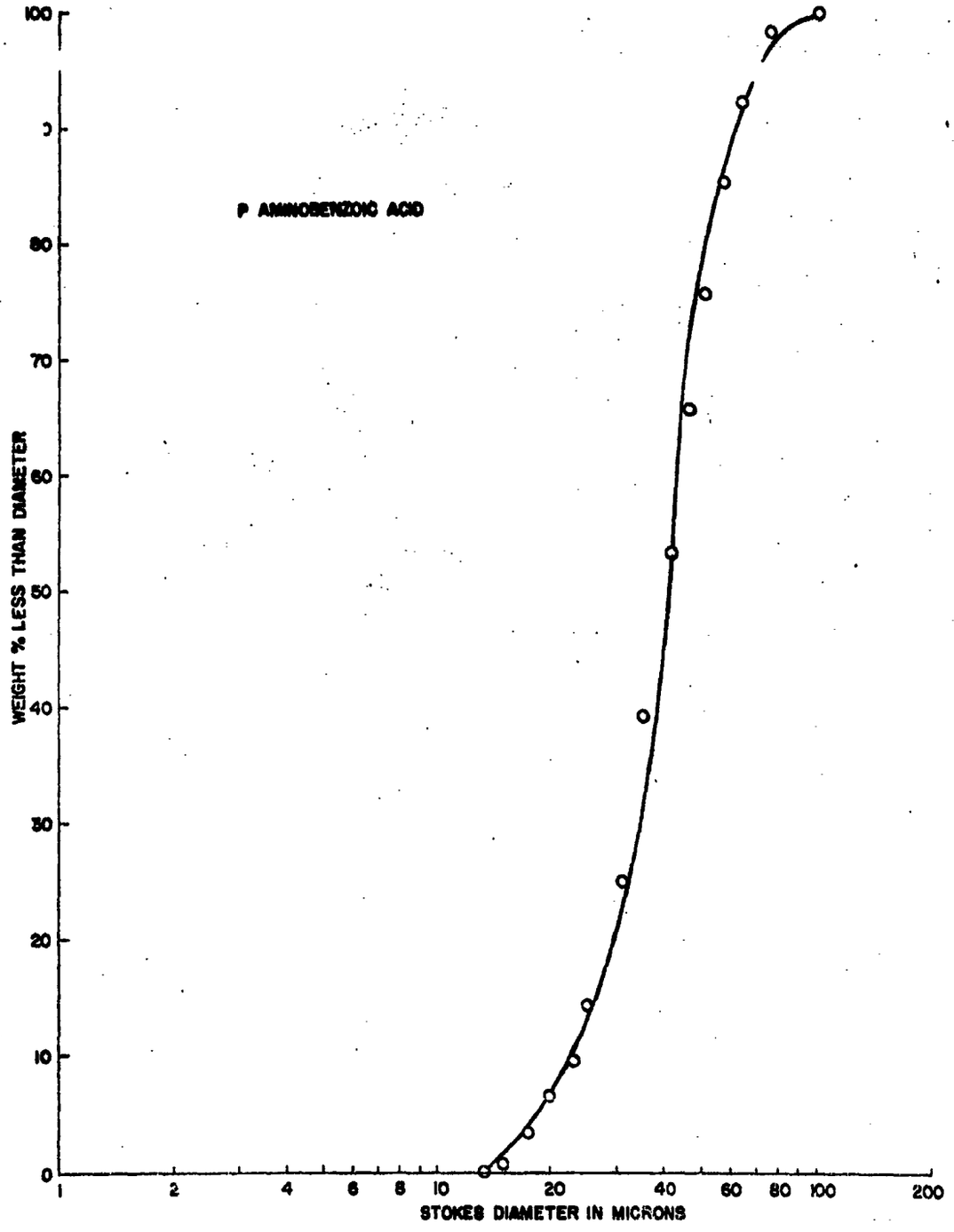

Figure 8. Particle-Size Distribution of Starting Material (p-Aminobenzoic Acid).

The same experimental details of firing and sampling were used in the case of organic materials and in the alum experiments. The sieve fractions and millipore filters were analyzed by ultraviolet spectrophotometry for p-aminobenzoic acid content (Appendix A). Results from the tests with organic materials are given in Table 5. The tracer data from these tests are shown in Figure 9.

In Figure 9, the resultant particle-size pattern again shows the apparent increase in particle size with distance from the high explosive charge up to a point. Then the particle size decreases again near the outer surface of the bomblet. Figure 10 illustrates the final size distribution of the total salt content of these bomblets.

3.2 EFFECT OF BOMBLET CASING VARIATION

Since the increased breakup in the outer layers of the spherical bomblets had been duplicated in several experiments, it seemed possible that the shockwave interactions at the outer surface as well as aerodynamic processes were the major influence on this breakup. Replacing the thin (0.010-in.) cellulose acetate with a more massive confining material changes the manner of shock passage to some degree since more energy will be required to breakup and move the heavier casing. Tenite-II plastic, already available in 3.0-in.-ID spheres with 0.0625-in.-thick walls, was the material chosen. The internal construction of the bomblets made from these thick-walled spheres was essentially the same as for the first group of experiments, except that the 3.0-in.-dia limitation permitted only four tracer positions rather than the original five. The same firing and sampling procedures as previously described were employed in these tests. The inert material was again potassium alum and the tracer, chrome alum. For direct comparison with these thick casing tests, four bomblets having the same structure but with 0.010-in.-thick cellulose acetate outer walls were tried. The data from these two sets of experiments are given in Table 6.

The final MMD of the total salt content vs average distance from high explosive-to-tracer, for thick- and thin-walled spheres, is plotted in Figures 11 and 12 respectively. There is no significant difference between test results obtained from bombs with thick and thin casings. Again, some deviation from the ideal horizontal line is evident. Figure 13 is a plot of all of the data points from the original design and the thick-and thin-walled 3.0-in.-dia spheres. For clarity, the average values determined in these tests are plotted in Figure 14.

Table 5. Experimental Data for Concentric Sphere Series (Organic)

Test	Tracer Charge Distance, Average (in.)	Total Salt		Tracer		Material Balance	
		Initial MMD (μ)	Final MMD (μ)	Initial MMD (μ)	Final MMD (μ)	Total	Tracer
60	All Inert	28.00	78	42	---	67.7	---
61	0.07	28.34	45	↓	53	101.0	135.0
62	0.32	29.63	53	↓	40	79.4	64.7
63	0.57	28.91	80	↓	104	93.0	88.6
64	0.82	35.30	44	↓	125	116.0	74.4
65	1.07	30.72	46	↓	55	104.0	95.9

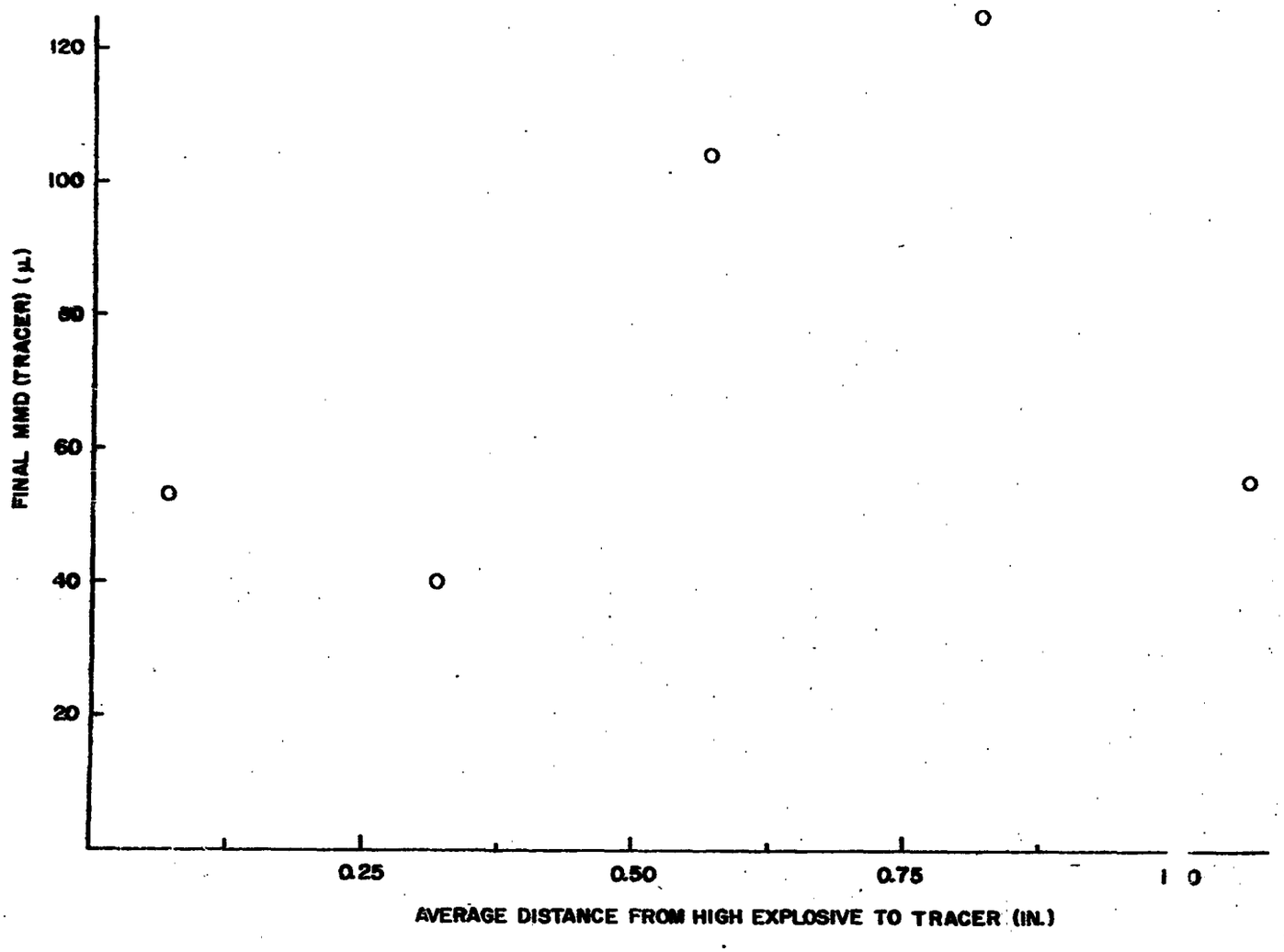

Figure 9. Plot of Tracer Breakup vs Radial Distance From Charge (Organic)

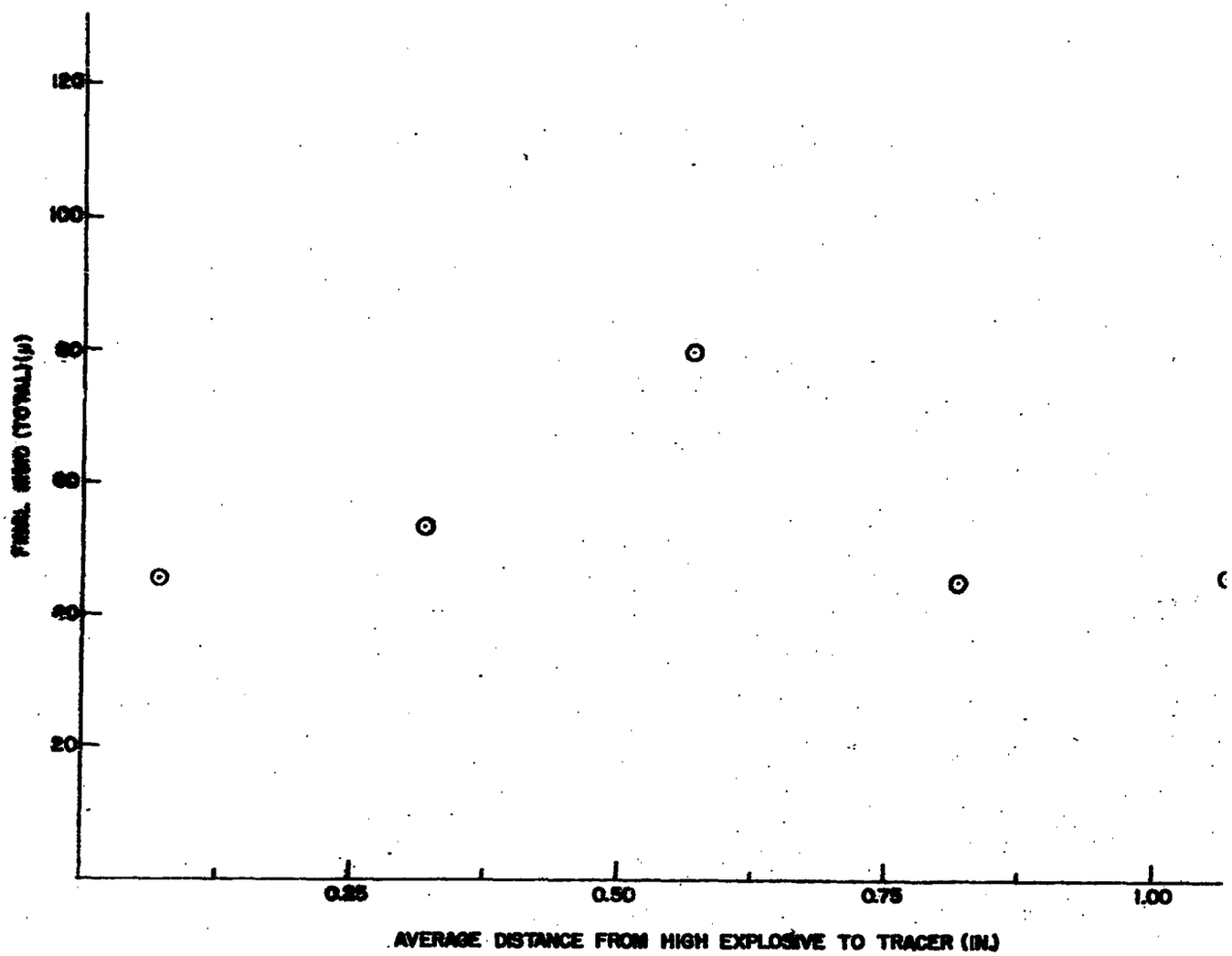

Figure 10. Variation of Resultant Gross MMD With Tracer Positions (Organic).

Table 6. Experimental Data for Concentric Sphere Tests (Casing Variation).

Test	Casing	Tracer-Charge Distance, Average (in.)	Initial MMD (μ)	Final MMD (μ)		Material Balance (%)	
				Total Salt	Tracer	Total Salt	Tracer
26	0.0625 in. Tenite II	0.82	665	174	147	84.5	66.8
27	↓	0.57	↓	145	98	74.1	102.4
35	↓	0.57	↓	150	235	64.4	72.6
28	↓	0.32	↓	137	139	59.2	57.9
29	↓	0.07	↓	129	62	71.0	105.1
17	0.010 in. Cellulose Acetate	0.82	↓	166	188	63.2	52.1
30	↓	0.57	↓	108	213	123.0	75.6
34	↓	0.57	↓	130	172	70.0	63.2
31	↓	0.32	↓	154	125	65.4	52.4
32	↓	0.07	↓	125	87	100.5	50.6

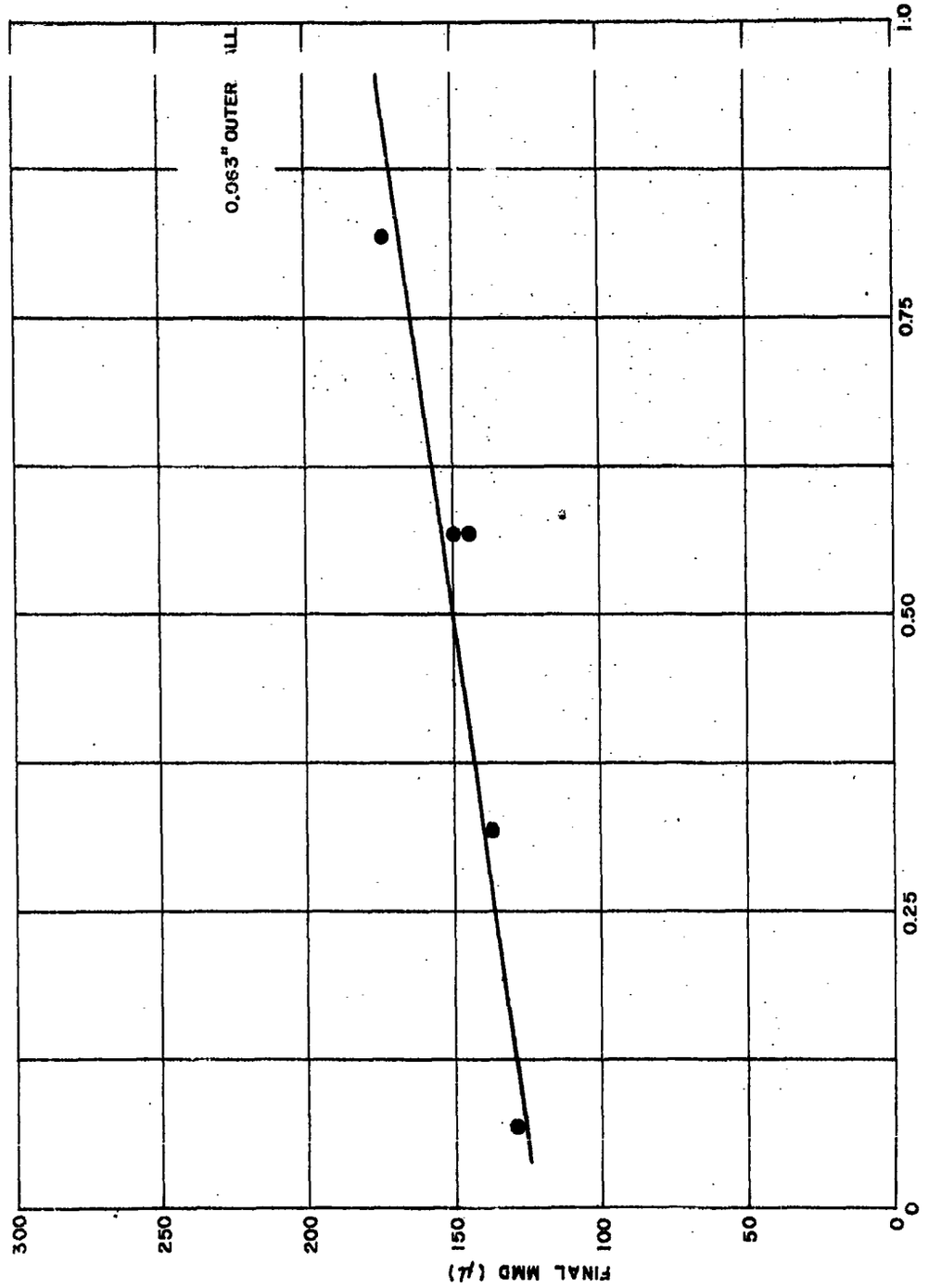

Figure 11. Breakup of Total Salt (Thick Wall).

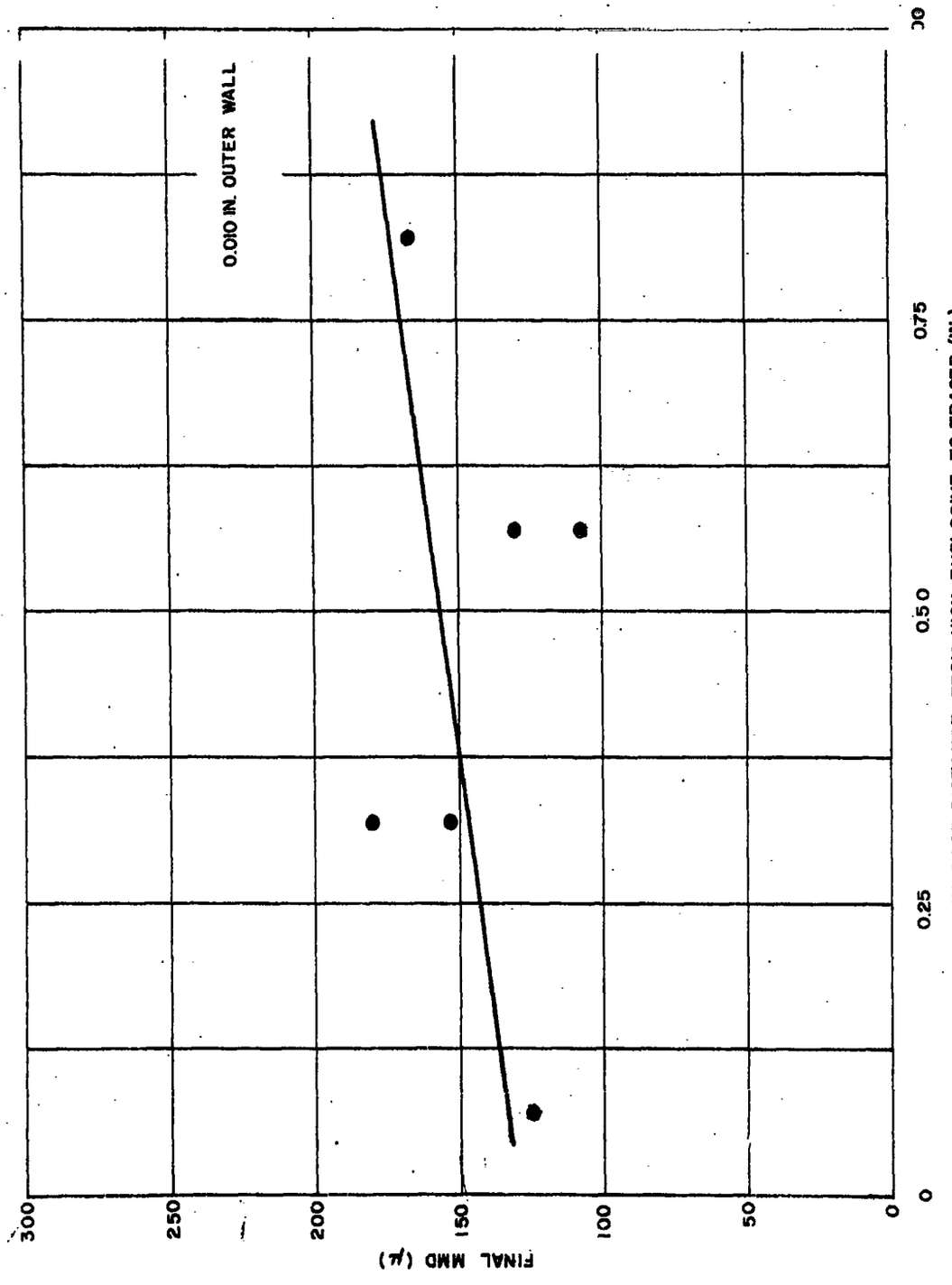

Figure 12. Breakup of Total Salt (Thin Wall).

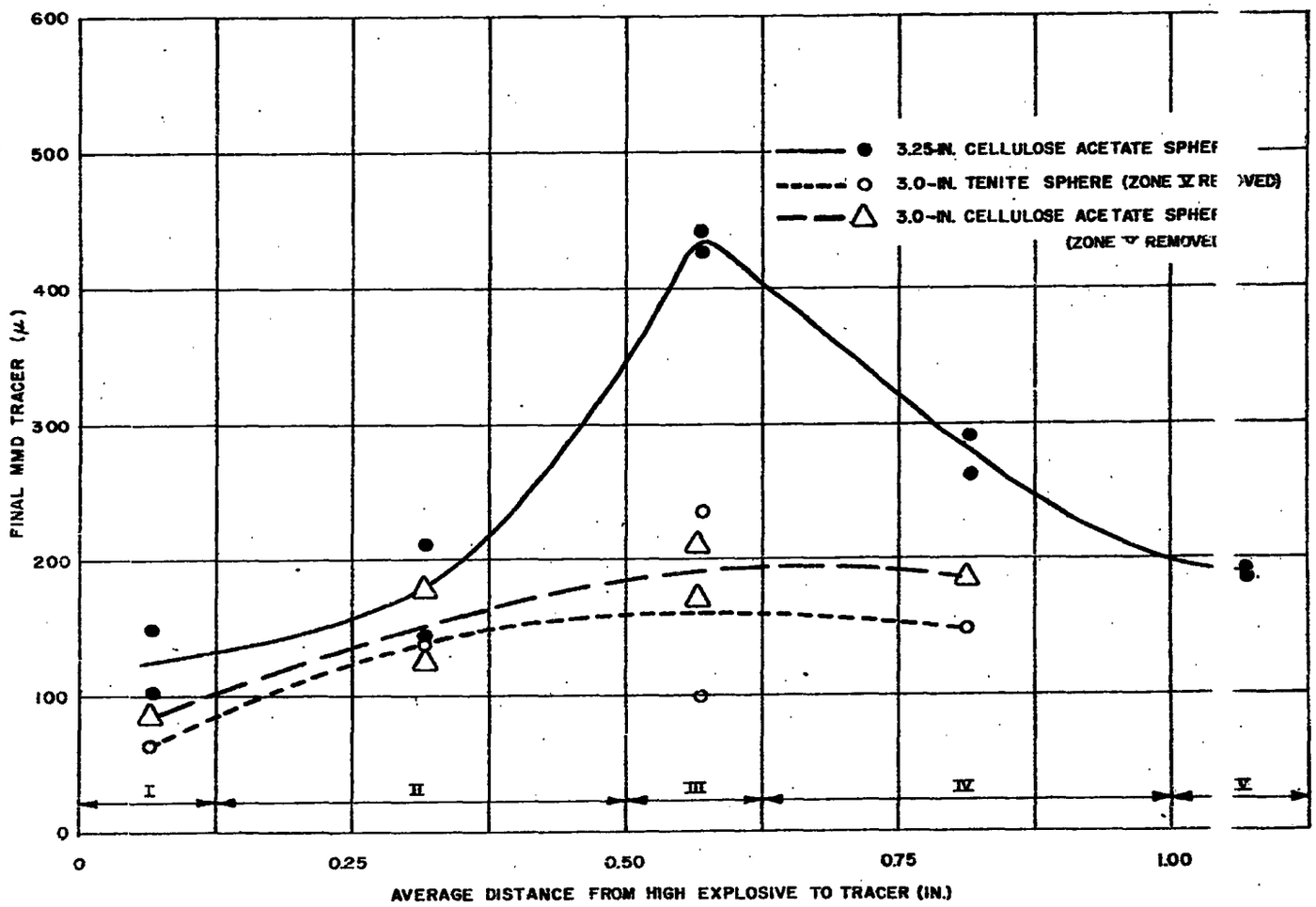

Figure 13. Tracer Breakup in Various Bomblet Types.

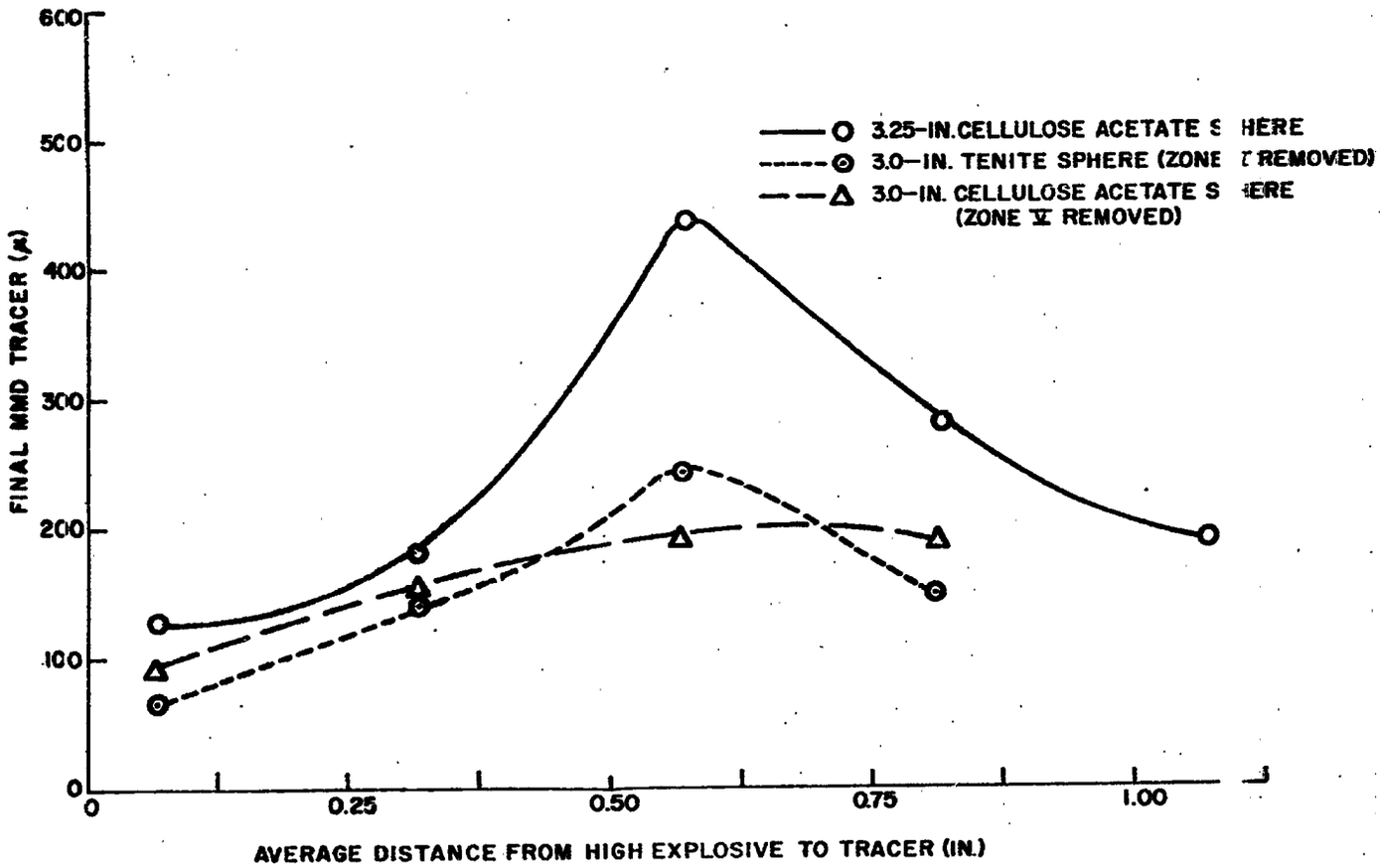

Figure 14. Average Tracer Breakup in Various Bomblet Types.

Improvements in the analytical procedure for chromium made possible the analysis of the millipore filters in some of these tests. Table 7 and Figure 15 present the data for the [illegible] indicate that the percentage of very small particles produced is highest in the layers near the explosive charge and is lowest at the outer surface. Evidence of this nature supports the theory that the very fine particles are a product of the evaporative effect of the hot detonation products.

3.3 LAYER STRIPPING EFFECTS

Since the general trend of results in the alum experiments is evident when the tracer layer is placed at various positions in a constant size bomblet, it is expedient to examine the effect of making each of these tracer layers an outer layer to determine whether this outer layer effect is a function of absolute size or of relative position. This was accomplished by running a series of experiments in which the breakup of tracer in the outer layers of successively smaller spheres was observed. The series of spheres was produced by sequentially stripping the outer layers from the standard concentric sphere device previously described.

Data from these experiments are shown in Table 8. Figure 16 is a plot of the data for total salt content of the layer-stripping devices. A comparison of the tracer data for the original concentric sphere series and the layer stripping series is given in Figure 17.

3.4 SHOCK AMPLIFICATION EFFECTS

Tests 8 and 9 (Table 3) apparently were not affected by the reduction of the hot detonation gases obtained by confining the explosive charge in a thick plastic chamber. Another series of experiments was conducted in which the explosive was confined in a metal chamber. A metal chamber should more effectively hold the hot detonation products and, in this design, should also allow the expanding explosive chamber a relatively free run before impacting the first salt layer, thereby increasing the peak shock pressure. This "free run" was provided by surrounding the explosive casing with an air layer surrounded by the alum layer.

Table 7. Samples Remaining Airborne at 27 Min.

Shot	Average Tracer-Charge Distance (in.)	Original Weight (gm)			Weight Airborne at 27 Min [Smaller than 9μ (gm)]			% of Origin Weight Airbo at 27 Min	ne
		Chrome Alum	Potassium Alum	Total	Chrome Alum	Potassium Alum	Total	Chrome Alum	T :al
29	0.07	10.3	270.8	281.1	0.177	4.15	4.33	1.72	1 54
28	0.32	52.2	221.9	274.1	0.185	1.79	1.97	0.36	0 70
27	0.57	23.3	244.4	267.7	0.198	2.95	3.15	0.27	18
26	0.82	188.7	85.6	274.3	0	3.54	3.54	0	29

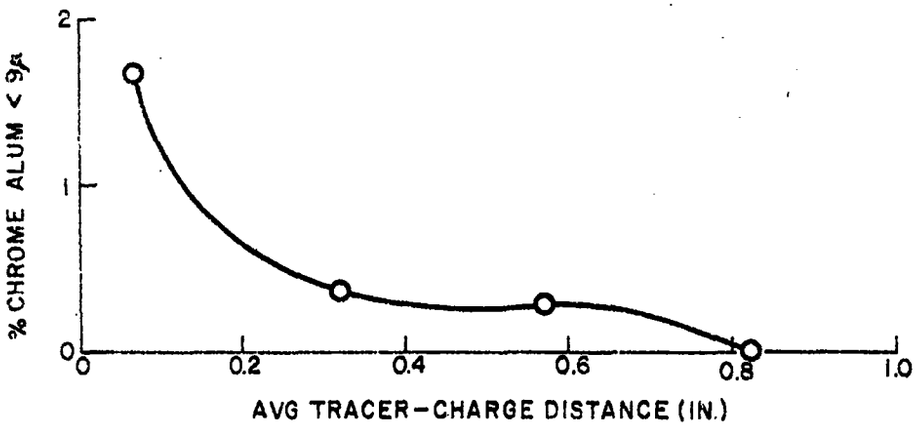

Figure 15. Amount of Fine Tracer Particles in Thick-Walled Bomblets.

Table 8. Experimental Data for Layer Stripping - Concentric Sphere Tests.

Test	Tracer-Charge Distance, Average (in.)	Initial MMD (μ)	Final MMD (μ)		Material Balance (%)	
			Total Salt	Tracer	Total Salt	Tracer
6	1.07	665	176	192	116.5	80.5
7	1.07		195	185	99.8	78.8
17	0.82		166	188	63.2	52.1
18	0.57		131	105	61.4	48.2
19	0.32		110	135	57.2	39.3
20	0.07		95	95	180.0	180.0

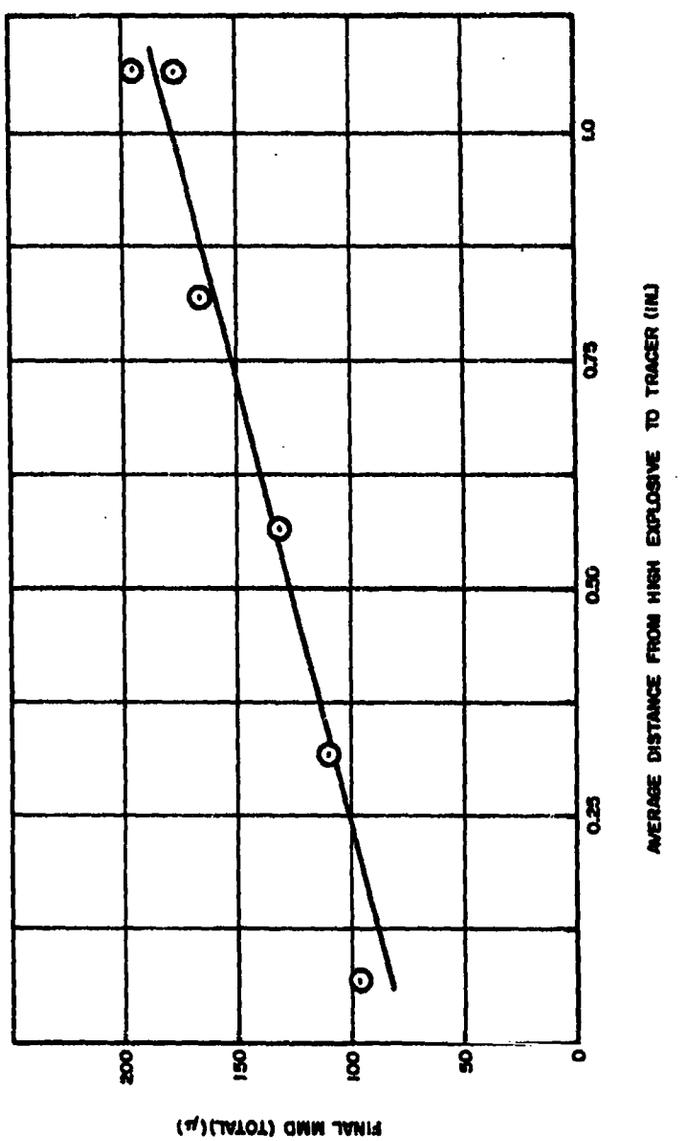

Figure 16. Particle Size of Salt vs Tracer Position (Series E-5b).

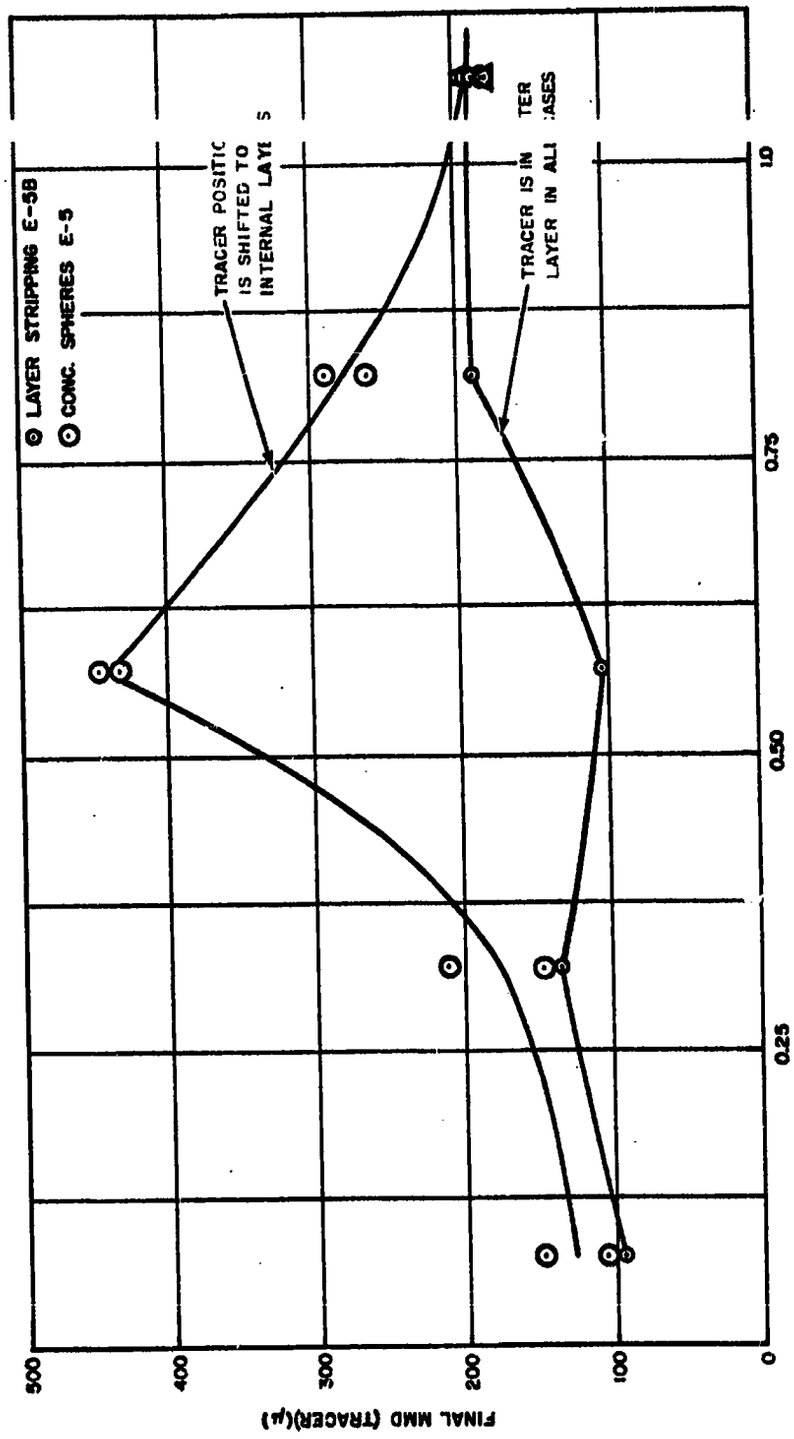

Figure 17. Comparison of Layer Stripping With Variable Tracer Position (Particle Size of Tracer vs Position).

Eleven tests were run in this study, using three conditions. Results of these tests are provided in Table 9.

The explosive chamber employed in the first series (Figure 18) consisted of a 0.250-in.-aluminum wall container with a 0.125-in. air gap. The remaining three spheres of the device were constructed of 0.010-in.-thick cellulose acetate. Similar devices were used in the second and third series, except that the metal explosive chambers employed a 0.063-in.-thick wall and four agent spheres (Figure 19). The explosive chamber employed in the second test series was made of aluminum, in the third series, copper. The explosive used in all three experiments was Aerex L-1 (Aerojet Liquid Explosive), detonated with a du Pont No. 8 detonator. Standard sedimentation, sieving, and chemical assay techniques were used to sample and analyze the resulting aerosol.

Figure 20 illustrates results obtained from the tracer analyses and compares these data with previously reported results of tests using standard plastic spheres. It is apparent that there is a tendency toward increased breakup in the outer layers of the spheres. As shown in Table 9, material balances are generally good for both the alum and the tracer.

Plots of total salt recovered in the devices are shown in Figure 21. If all salt layers were identical, the illustrated curves would be horizontal; there is, however, a slight variation from this ideal slope. The points on the curves for the thin-walled shots show little deviation (indicating good reproducibility). A slightly greater breakup was produced with the aluminum than with the copper.

Results of the thick-walled shots show a somewhat greater variation. It was noted that both types of aluminum chamber fractured into many relatively small pieces while the copper vessels generally produced a few large sheets (< 10). This result indicates that the copper stretched much more than the aluminum and was thus more likely to impart a uniform high-amplitude shock.

Results of tests using the two types of metal generally appear to be quite similar, with the exception of data from the layers nearest the plate impact. If this difference is significant, it could be accounted for by differences in shock characteristics, or by increased effects of escaping hot detonation gases in the aluminum liners.

Table 10 presents results from tracer assays of millipore filters and provides weights of small particles (>12 μ) produced by these devices.

Table 9. Results of Shock-Amplification Experiments.

Test	Series*	Average Explosive-to-Agent Distance (in.)	Initial MMD (μ)	Final MMD		Material Balance	
				Total (μ)	Tracer (μ)	Total (μ)	Tracer (μ)
40	1	0.75	665	100	149	71	47
41	1	1.00		132	108	63	53
42	1	0.50		163	334	56	62
44	2	0.25		114	152	105	76
45	2	0.50		124	274	99	80
46	2	0.75		130	145	89	64
47	2	1.00		154	134	96	68
48	3	0.25		151	260	102	85
49	3	0.50		158	290	95	88
50	3	0.75		183	192	79	68
51	3	1.00		188	141	58	52

*Series 1: 0.250-in. aluminum wall
Series 2: 0.063-in. aluminum wall
Series 3: 0.063-in. copper wall

Table 10. Small Particles Produced by Pressure-Amplification Tests.

Test	Series *	Average Explosive-to-Agent Distance (in.)	Amount of Tracer Airborne at 19 Min (mg)	% of Original Tracer <12μ
40	1	0.75	24**	0.03***
41	1	1.00	45**	0.22***
42	1	0.50	0**	0.00***
44	2	0.25	49	0.22
45	2	0.50	115	0.25
46	2	0.75	78	0.13
47	2	1.00	49	0.03
48	3	0.25	98	0.42
49	3	0.50	652	1.26
50	3	0.75	152	0.22
51	3	1.00	685	0.35

*Series 1: 0.250-in. aluminum wall
Series 2: 0.063-in. aluminum wall
Series 3: 0.063-in. copper wall

**Airborne at 27 Min
***% <10μ

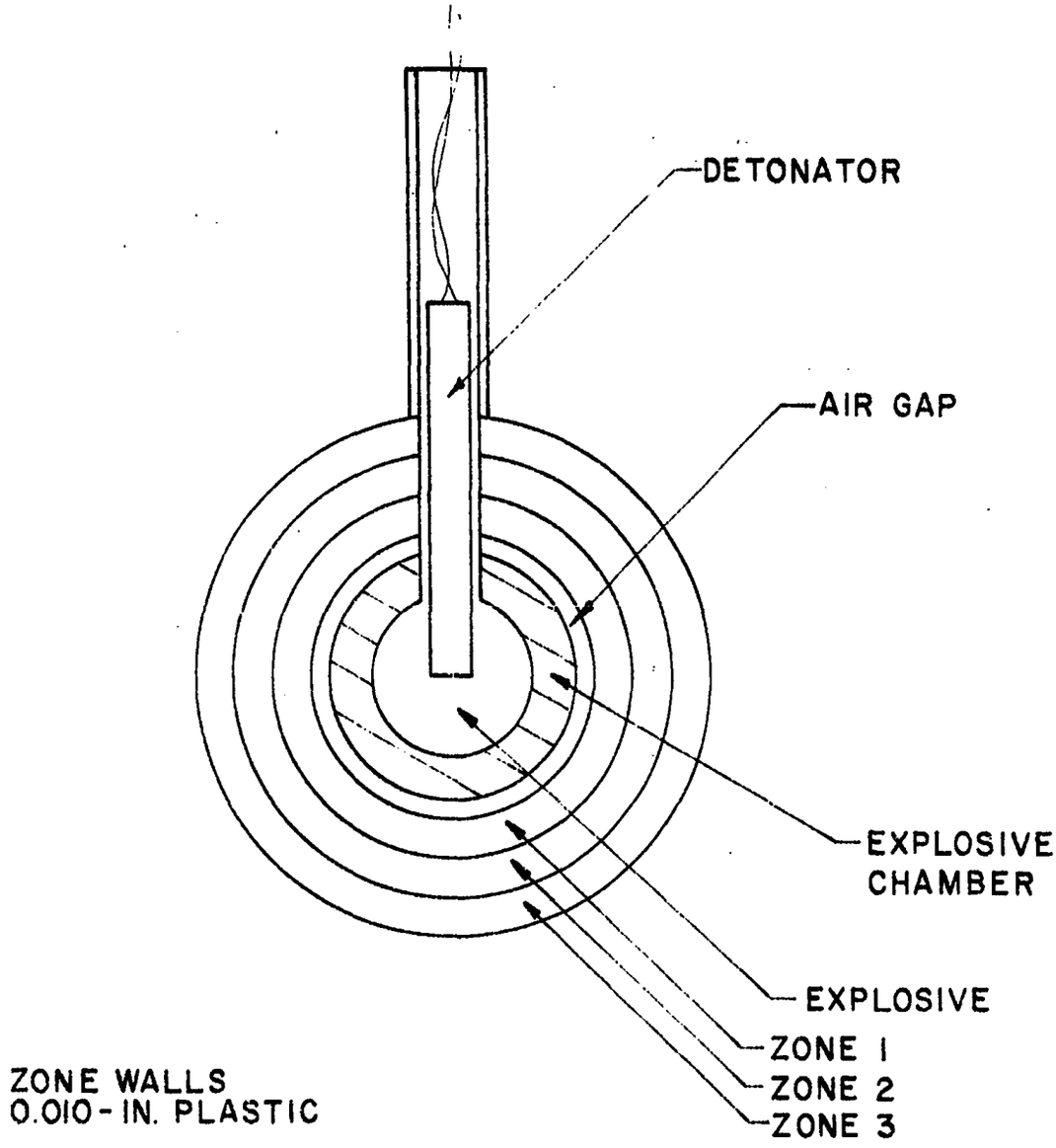

Figure 18. Shock-Amplification Device (1).

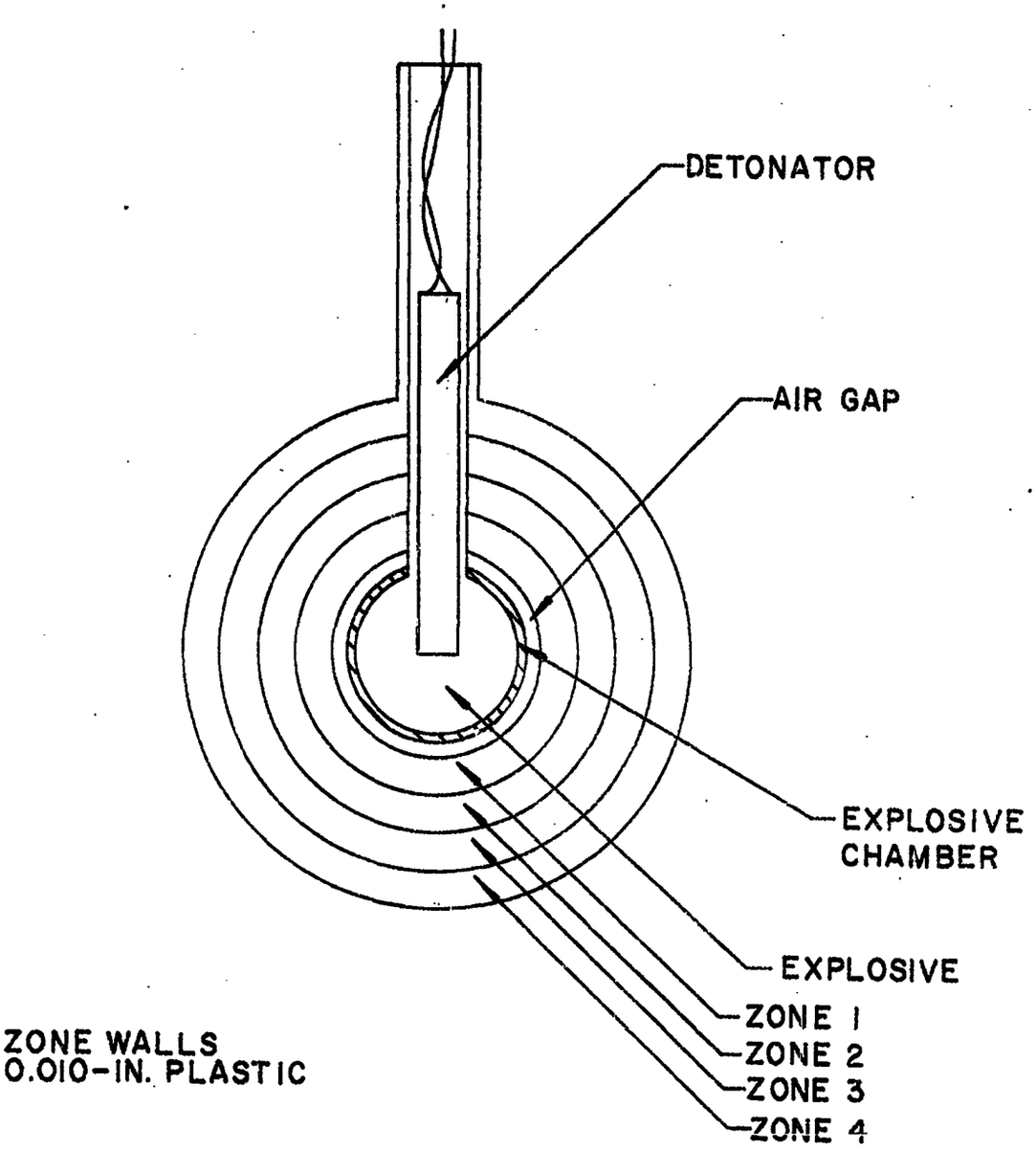

Figure 19. Shock-Amplification Device (2).

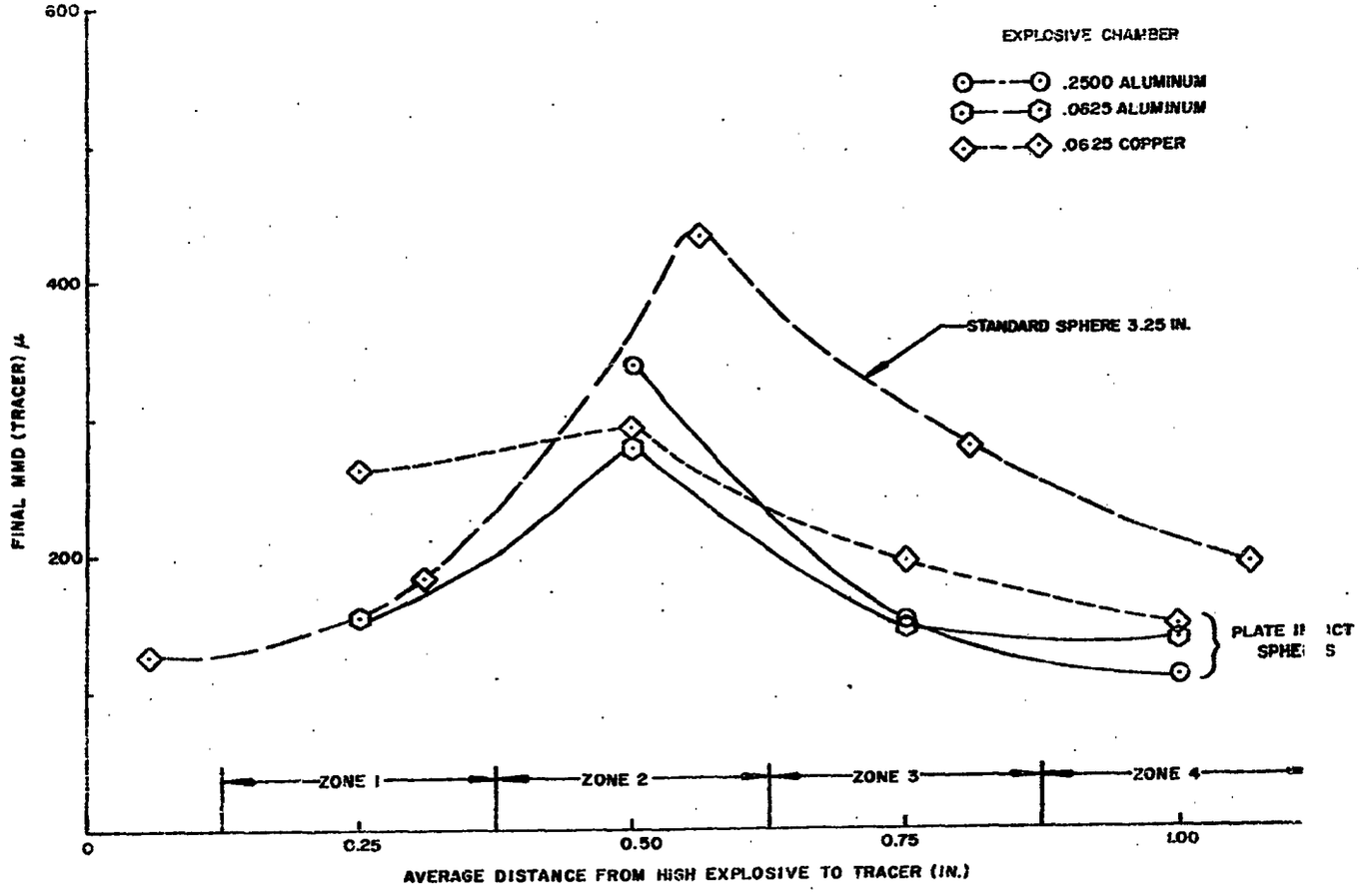

Figure 20. Tracer MMD of Radial-Effect Tests.

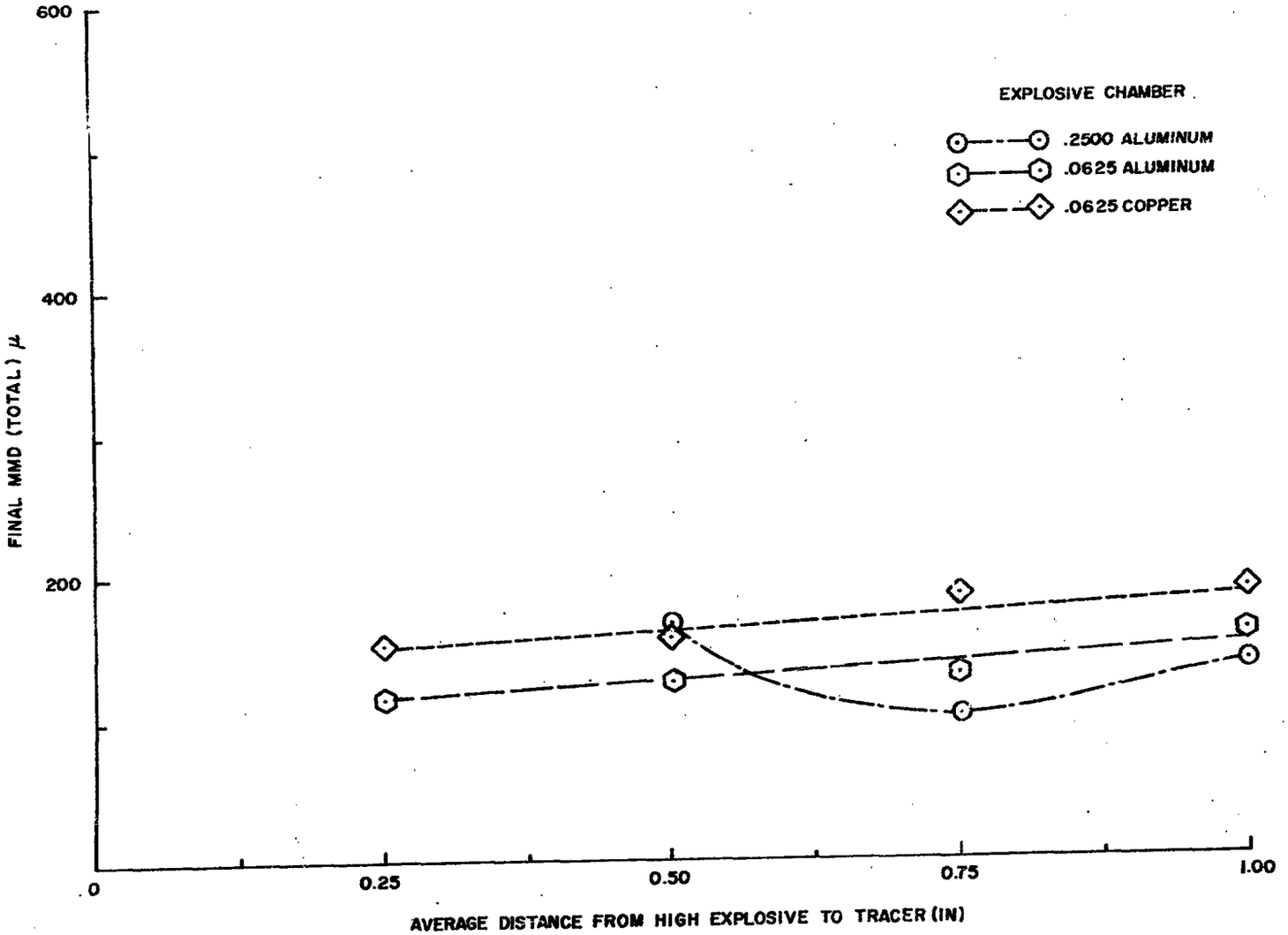

Figure 21. Total Salt MMD of Radial-Effect Tests.

As shown in Figure 22, very few small particles are formed in this process (<2%). Because the absolute amount of particles produced is small, the variation between the experiments is not considered

the same amount of small particles (Figure 15).

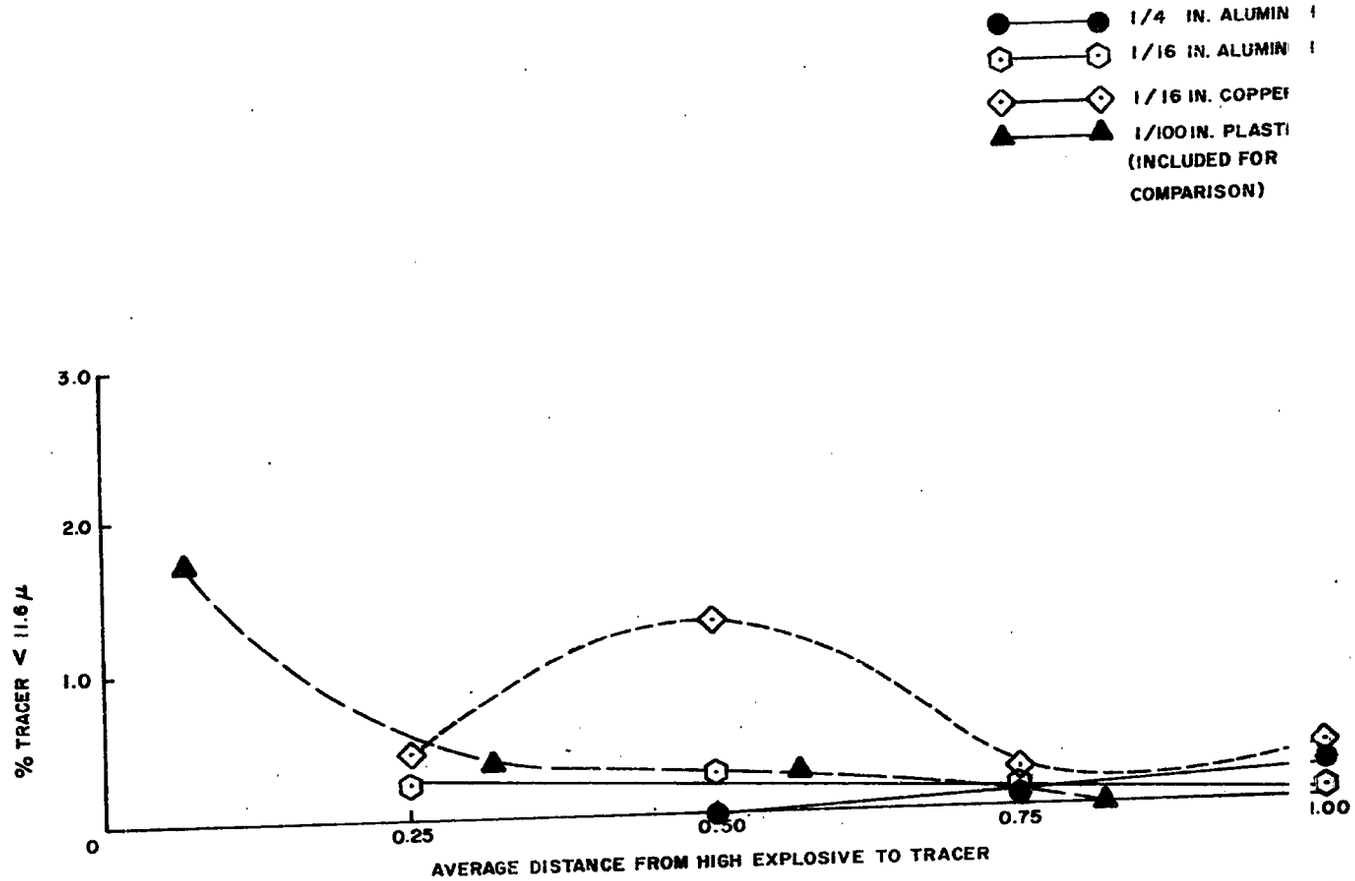

Figure 22. Small Particles Produced in Radial-Effect Tests.

4. ANALYSIS OF RESULTS

Results from the primary group of experiments in this series indicate that, for inorganic materials such as alum, a reduction in particle diameter is achieved when these materials are explosively disseminated.

The resulting MMD's of particles in these tests were reduced by two-thirds to three-fifths. Reducing the agent-to-burster ratio from 28:1 to 0.91:1 results in a further breakup of the total salt to one-seventh of its original MMD as shown in Figure 23. This small increase in size reduction with a large increase in explosive-to-agent weight ratios indicates the low efficiency of breakup of relatively small particles in explosive dissemination devices.

The tests conducted with organic materials (p-aminobenzoic acid and anthraquinone) resulted in no decrease in particle size and generally showed an increase. It is probable that some fracture did occur in these cases but the competing reagglomeration mechanism was sufficient to result in a net increase in average particle size.

The tracer breakup-vs-distance from explosive charge investigation produced trends which were similar for both inorganic and organic materials. In both cases maximum resultant particle sizes were obtained in the intermediate layers of the bomblets. In the case of the inorganic agents however, there was a net reduction in size of particles. In the case of the organic agents there was a net increase in size. This trend was obtained by using both the total salt and the tracer alone for organic materials. The organic material, which had an initial MMD of $\sim 30\,\mu$, is in the particle size region described by Mac Lean (Reference 8) where inorganic materials (silica, glass) are very susceptible to agglomeration, and where some of the original particles may be disseminated without fracture. If the size increase is less at the explosive charge surface and at the outer surface of the device, as the experiments indicate (Figure 9), the final agglomeration is mainly produced in the central area of the agent section. The magnitude of the increased breakup (or decreased agglomeration) noted in the outer layers of agent and in those immediately surrounding a charge is experimentally significant as demonstrated by duplication of runs (Figures 1, 2, and 3).

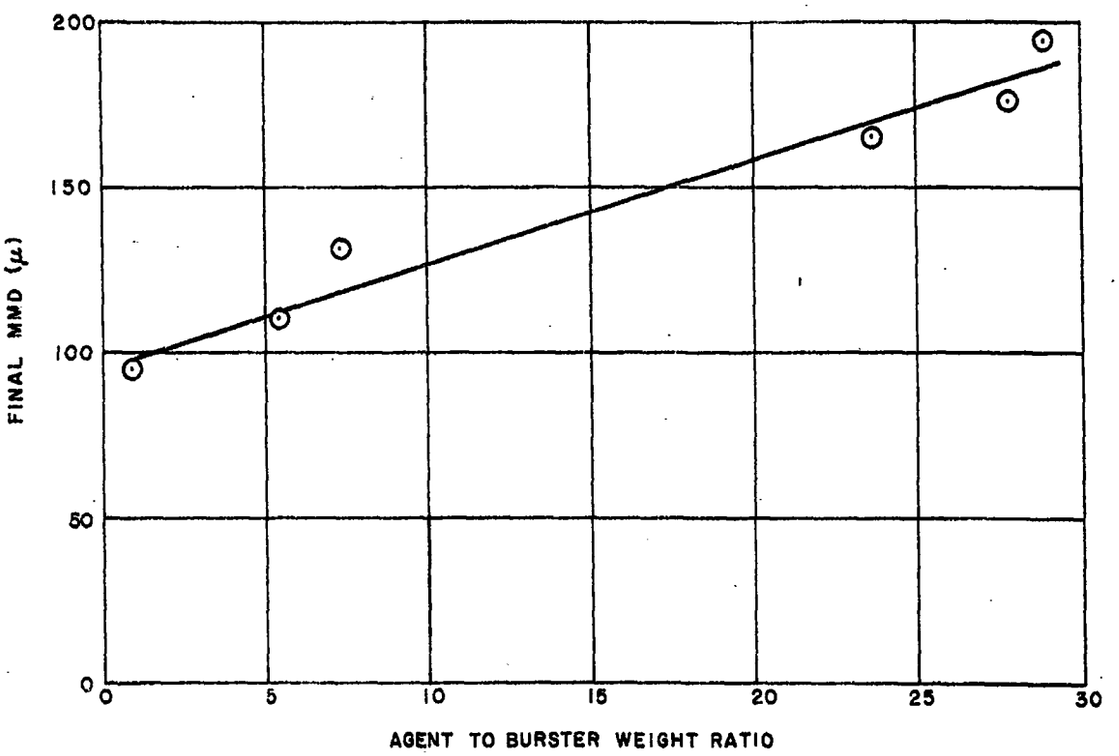

Figure 23. MMD Total Salt as a Function of Agent-to-Burster Ratio.

5. CONCLUSIONS AND RECOMMENDATIONS

systems, in the case of solid materials, should be designed to take advantage of their dissemination potential rather than their particle comminution function. It should be noted that, due to the consequent agglomeration of very fine particles, it may be necessary to presize the agent load several times smaller than the desired final effective size.

The mass fraction of particles in the small size ranges, i.e., those physiologically effective (materials below 10 μ dia), was very low in all the tests, generally less than 10% and usually less than 5% of the total. These results along with the low fracture efficiency tends to support the conclusion that presizing of the solid agent to smaller than the desired size range and reducing agglomeration effects would be the most effective means of employing an explosive dissemination device.

Although the exact nature of the mechanisms responsible for the "radial breakup profile" across a spherical bomblet has not been determined, the profile was demonstrated to exist and a technique for quantitatively describing it was developed. It is anticipated that this technique will be applicable not only in determining breakup characteristics described here, but also, with methods such as infrared and ultraviolet absorption spectrophotometry and gas-liquid chromatography, to decomposition studies of agents and simulants.

REFERENCES

1. Explosive Dissemination of Liquid Agents, Stanford Research Institute, series of reports on Contract No. DA-18-108-CML-5510 and DA-18-108-405-CML-261.

2. George Washington University, Research Laboratory, Final Progress Report, DA-18-064-CML-163, January 1, 1959.

3. A Series of Static Tests of Single Bis and VX-Filled 8-in. Shell Equipped with Agent-to-Burster Ratios of 2/1 and 23/1, and Detonated on the Ground at Various Heights, CWL Technical Memorandum 33-16, 10 December 1958.

4. Buck, D., The Explosive Dissemination of Liquids of Low Volatility, CWL Special Publication 1-7, Status Report August 1959.

5. Research Study on the Dissemination of Solid and Liquid Agents, Aerojet-General Quarterly Progress Report 0395-04(01)QP, July - September 1962.

6. Research Study on the Dissemination of Solid and Liquid Agents, Aerojet-General Quarterly Progress Report 0395-04(03)QP, January - March 1963, p. 11.

7. Buck, D., Explosive Dissemination of Low-Volatility Liquids from Cylindrical Devices, CRDLR 3038, January 1961.

8. Temperley, H. N. V., "Further Study of the Dispersal of Drops of Liquid By an Explosive Charge". Final Report, Directorate of Chemical Defense Research and Development, November 10, 1955.

APPENDIX A

ASSAY PROCEDURES

A1. DETERMINATION OF CHROMIUM IN AEROSOLIZED CHROME ALUM

The explosive dissemination of chrome alum described in this report resulted in a series of samples ranging from Millipore filters holding microgram quantities of chromium to sieve fractions with gram amounts.

The analytical procedure used consisted essentially of three steps: (1) Extraction of salt from the millipore filter or sieve sample, (2) oxidation of trivalent to hexavalent chromium, and (3) spectrophotometric determination of the hexavalent chromium in the form of the red-violet complex which it forms on reaction with 1, 5-diphenylcarbohydrazide (s-diphenylcarbazide).

Procedure:

Weigh out sufficient sample to contain ~ 2 to 10 μgm of chromium per milliliter of sample solution. Disolve the sample in 5% sulfuric acid and make up to 100.0 ml with the acid. Heat a 5.0 ml aliquot with 10 ml of 2% ammonium persulfate on a boiling water bath for 20 min. Dilute the heated samples to ~40 ml and make neutral to methyl orange with a 10% solution of sodium hydroxide, using an outside indicator. Add 3.3 ml of 1:5 sulfuric acid to the solution and transfer to a 100 ml volumetric flask with distilled water. Add 1.0 ml s-diphenylcarbazide solution (4.0 gm phthalic anhydride and 0.25 gm s-diphenylcarbazide q.s. to 100 ml with 95% ethanol) to the flask and dilute to the mark (100 ml) with distilled water. Read the maximum color development of the solution in a Klett-Summerson photoelectric colorimeter with a No. 54 filter (~6 min after the addition of the diphenylcarbazide solution). Run reagent blanks with each set of determinations.

Run standard solutions in the same concentration range with each set of determinations and compare the unknown readings with the standard. A typical absorbance/concentration curve obtained with this method is shown in Figure A1.

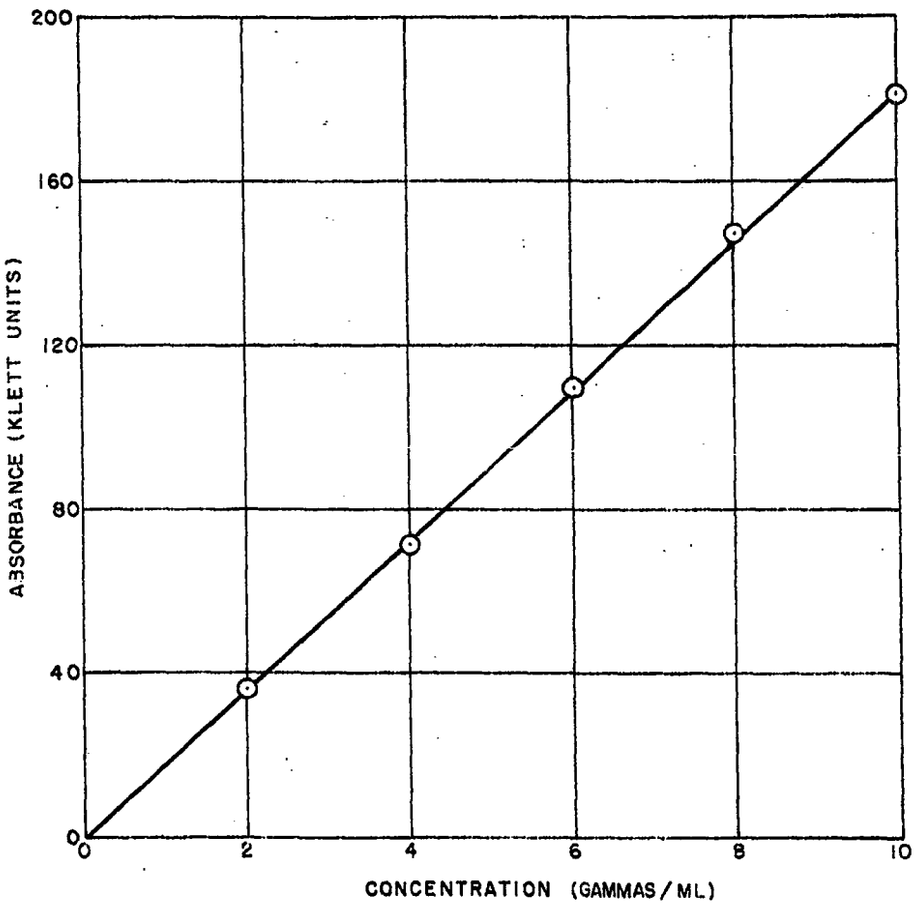

Figure A1. A Standard Colorimetric Curve for Chromium.

A2. SPECTROPHOTOMETRIC DETERMINATION OF p-AMINOBENZOIC ACID

The ultraviolet absorption spectrum of p-aminobenzoic acid in aqueous solution shows a maximum at 266 mμ. The anthraquinone associated with it in these tests has no significant contribution to this absorbance.

Procedure:

Weigh out sufficient sample to contain ~ 5 μgm of p-aminobenzoic acid per milliliter of final solution. Disolve the sample in distilled water and read the absorbance of the solution directly at 266 mμ using a distilled water blank. Compare the readings with those of a standard in the same concentration range.

Typical absorbance and concentration curves obtained with this method are shown in Figures A2 and A3.

A3. INERT SPECIES

The general procedure for determining the amount of inert material in a given sample is to chemically determine the amount of tracer as described above and subtract this weight from the total weight of the sample. The difference is taken as the weight of the inert species.

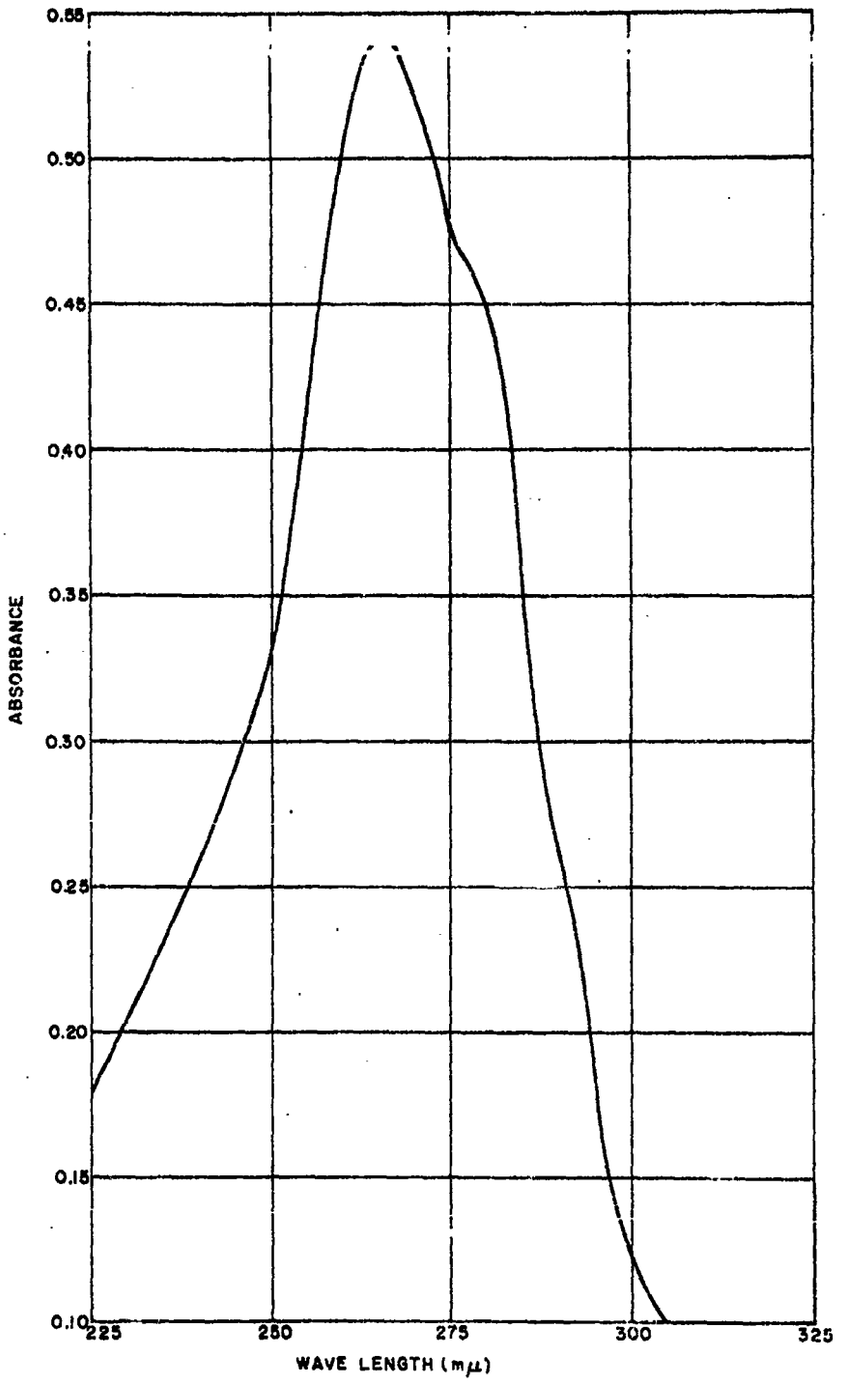

Figure A2. Ultraviolet Absorption Spectrum of p-Aminobenzoic Acid.

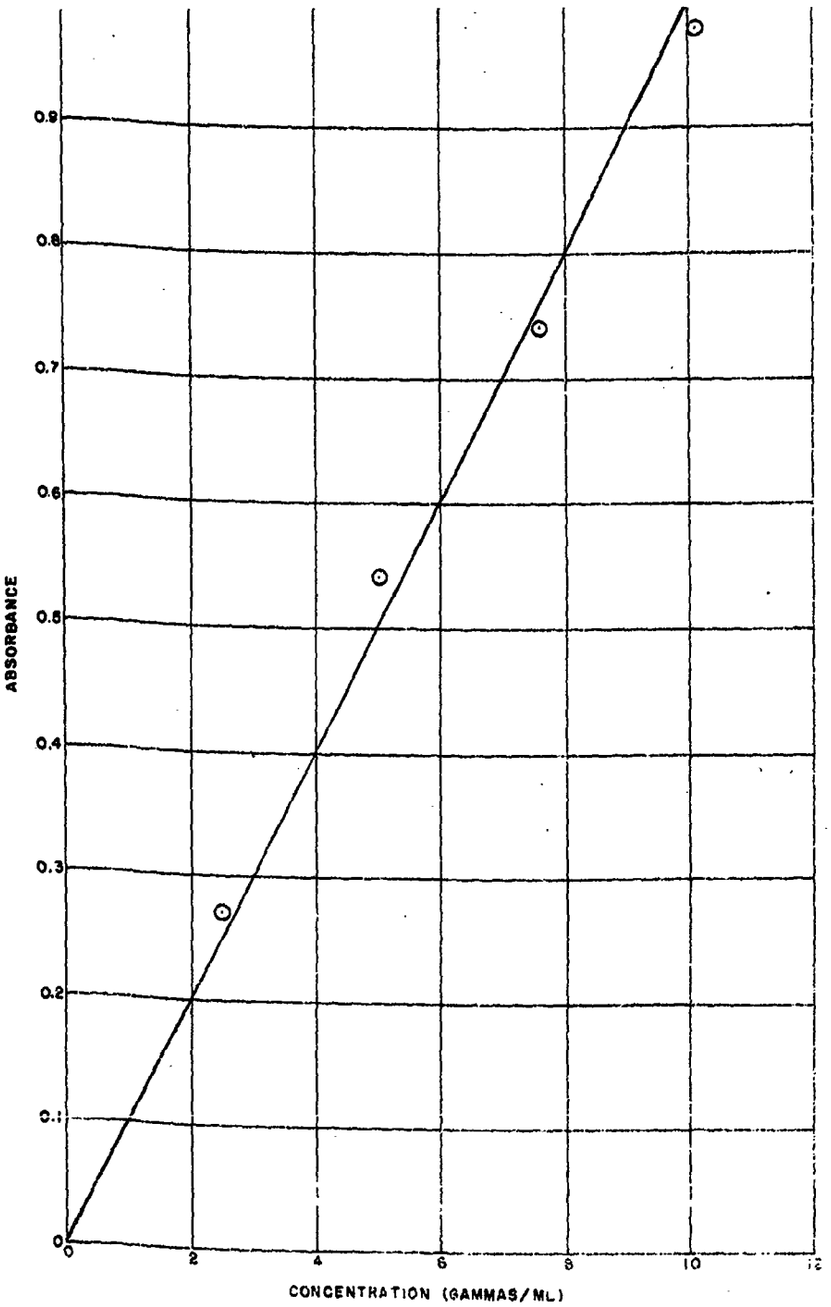

Figure A3. Standard Absorbance Concentration Curve for p-Aminobenzoic Acid.

ACKNOWLEDGEMENT

The assistance of Mr. K. L. Harris on the chemical analysis phase of this program is gratefully acknowledged.